Results in Control and Optimization 19 (2025) 100572

Contents lists available at ScienceDirect

Results in Control and Optimization

journal homepage: www.elsevier.com/locate/rico

Addressing ORPD problem in a standard IEEE power network accompanied with RESs and FACTs appliances by COMMKE under volatile load scenarios

Susanta Dutta [a,1], Tushnik Sarkar [a,1], Chandan Paul [a,1], Sabbir Reza Tarafdar [b,1], Provas Kumar Roy [c,1], Ghanshyam G. Tejani [d,e,1], Seyed Jalaleddin Mousavirad [f,*,1]

[a] Department of Electrical Engineering, Dr. B.C. Roy Engineering College, Durgapur, India
[b] Department of Computer Science and Engineering, Dr. B.C. Roy Engineering College, Durgapur, India
[c] Department of Electrical Engineering, Kalyani Government, Kalyani, West Bengal, India
[d] Department of Research Analytics, Saveetha Dental College and Hospitals, Saveetha Institute of Medical and Technical Sciences, Saveetha University, Chennai, 600077, India
[e] Applied Science Research Center, Applied Science Private University, 11937, Amman, Jordan
[f] Department of Computer and Electrical Engineering, Mid Sweden University, Sundsvall, Sweden

ARTICLE INFO

Keywords:
Optimal reactive power dispatch (ORPD)
Renewable energy sources (RESs)
Chaotic oppositional multi-trial vector based monkey king evolution (COMMKE)
Thyristor switch capacitor (TSC)
Thyristor controlled reactor (TCR)

ABSTRACT

This research examines the optimal reactive power dispatch (ORPD) problem across IEEE 30 & 118 bus experimental networks. In particular, we incorporate renewable energy sources (RESs) like solar photovoltaic (PV) and wind power (WP) into the conventional network after first balancing it. Both singular and multiple objective functions (OFs) are considered here. These are, both alone and together, a drop in aggregated voltage deviation (AVD) over buses and a reduction in active power loss (APL). Twenty one cases in all have been looked at using three test frameworks. TSC-TCR (FACTs devices) with test setup are being used for cases 4–6, 9–12 & 16–21. The objectives have been achieved by the use of the COMMKE algorithm, a multi-trial vector-based monkey king evolution (MMKE) method integrated with oppositional based learning (OBL) and chaotic based learning (CBL). Comparative analysis has also been done on the performance of the other optimization methods that were showcased in the latest ORPD research. Both constant and dynamic load demand scenarios are covered in the study. Appropriate probability density functions (PDF) are used to forecast the uncertain WP, PV source, and load demand. Uncertain situations with fluctuating load demand, wind speed (WS), and sun irradiation (SI) are simulated using Monte Carlo simulations (MCS). The investigations' findings demonstrate that, in a variety of cases, the COMMKE outperforms optimization techniques found in the recent ORPD literature. The improvement of power network efficiency in ORPD difficulties by the application of TSC-TCR is another noteworthy conclusion. To scrutinize the performance of COMMKE, the identical experiments have been conducted using MMKE & driving training based optimization (DTB) and the results coming from COMMKE, MMKE & DTBO are compared. To make this comparison more lucid, statistical records are produced, box plots are presented, error bar plots are used and moreover one way ANOVA test has been performed over the results generated through the different optimization approaches.

* Corresponding author.
E-mail address: seyedjalaleddin.mousavirad@miun.se (S.J. Mousavirad).
[1] All authors contributed equally.

https://doi.org/10.1016/j.rico.2025.100572
Received 21 March 2025; Received in revised form 22 April 2025; Accepted 3 May 2025
Available online 22 May 2025

1. Introduction

The rapid load growth substantially leads the power systems runs under stressed operating condition. Alongside the increase in load rise of power systems, there has been a significant negative trend in greenhouse gas emissions. This is because classical power plants that use fossil fuels are utilized more frequently, resulting in greater emissions, and more electricity is needed to fulfill the expanding demand. This has a negative effect on the ecosystem and exacerbates other environmental problems like global climate shift. To avoid the detrimental impacts of load hikes on greenhouse gas emissions, power systems must include clean and renewable energy sources, such as solar and wind, in their producing mix. They do not affect greenhouse emissions in the atmosphere [1]. On the other hand, scholarly and business communities have recently paid close attention to RESs, especially PV source & WP. Managing the unpredictable and intermittent nature of RESs, including solar and wind, has grown increasingly difficult as more are included into the power grid [2]. For the system to remain stable and manage fluctuations in electricity generation and demand, the power system must be adaptable enough [3].

Moreover, transmission systems with increased loading and smaller capacity margins are intended to be moved by power system operators, who are responsible for growing load demand. Voltage stability is a critical issue in the functioning of a power system due to the new transmission system's increasing workload. Voltage stability is a vital component of power system performance, defined as the capacity of a power system to sustain a stable voltage profile during both normal and abnormal operating conditions. When a power system experiences load growth – a gradual increase in the amount of energy required – voltage stability plays a crucial role [4].

The electricity transmission and distribution networks must operate profitably and efficiently in order for ORPD strategy to be implemented. Researchers in power system strategy and execution have focused their emphasis on finding a solution to the ORPD challenge. The security, dependability, and financial operations of the system depend heavily on the solution of the ORPD. This is because it helps the network's voltage stay within acceptable ranges by supporting machinery that modifies reactive power flow when it is properly coordinated [5,6].

The purpose of the ORPD algorithm is to minimize a chosen objective function, such as voltage variation, actual power transmission losses, and the voltage stability index. These problems result from the increasing complexity of grid upgrading. In order to help sustain the voltage level at various loading states, ORPD is essential in lowering voltage deviation and power quality problems brought on by variations in electrical power [7].

The modification of the system control variables under various operational limitations, the intended objective function is accomplished. The ORPD problem is classified as a complex nonlinear problem due to its nonlinear objective function and various constraints in the context of mathematical model optimization [8].

Finding the best answers to the ORPD dilemma could be more challenging that strike a balance between affordability, dependability, and environmental sustainability if thermal generators are the sole option. Planning and optimizing power systems may be done more thoroughly and robustly by incorporating unpredictable RESs like solar and WP. The RERs particularly, wind turbines (WTs) and solar PVs are often integrated into electrical power networks. Nevertheless, the integration of WTs and solar PV systems is beset by their stochastic character as well as inconsistent wind and SI behavior [9]. These unpredictable resource natures can lead to variations in the performance of the electrical network, so it is crucial to manage the varying demand for power and uncertain behavior in order to address the ORPD problem [10].

A significant number of scholars have investigated the ORDP problem using classic optimization techniques, particularly in systems that incorporate orthodox thermal units such as Newton method [11], the interior point method [12,13], linear programming (L.P.) [14,15], nonlinear programming [16], and quadratic programming (Q.P.) [17–19]. The need for continuous and differentiable objective functions and the tendency to enter local optima are often disadvantages of these methods. Therefore, it became imperative to devise novel approaches to surmount these limitations. The global or nearly global optimal solution to the ORPD issue cannot be found by these. Furthermore, by taking into account theoretical presumptions such ORPD's convexity, continuity, and differential nature, these strategies are applied to solve the ORPD issue.

Therefore, new approaches have to be developed in order to get around these problems. One efficient technique for resolving optimization problem is the meta-heuristic algorithm (MA) [20]. Researchers are using MAs more frequently because of their accessibility and straightforward ideas. The introduction of MAs has increased the options available for resolving the ORPD issue. Swarm intelligence (SI)-based, evolutionary technique-based, and physics-based MAs may be separated into three groups. The ORPD problem has been solved using a number of MAs, including the improved slap swarm algorithm [21], barnacle mating algorithm [22], slime mould algorithm (SMA) [23], two-archive multi-objective grey wolf optimizer (2ArchMGWO) [24], improved grey wolf optimizer [25] artificial bee colony algorithm [26], hybrid PSO and gravitational search algorithm (PSOGSA) [27], and particle swarm algorithm (PSO) [28,29].

With the emergence of computational intelligence, numerous single objective evolutionary algorithms (E.A.s) get developed and evaluated to address non-convex, nonlinear ORPD optimization problems, typically associated with conventional heat generators. These include quasi-oppositional differential evolution (QODEA) [30], modified GAME theory [31], artificial bee colony with firefly (ABC-FF) [32], artificial bee colony (ABC) [33], quasi-oppositional differential optimization (QOTLBO) [34,35], ant colony optimization [36], hybrid imperialist competitive algorithm (ICA), teaching learning-based optimization (TLBO) [37], hybrid ICA-PSO [38], history-based adaptive differential evolution (SHADE) [39], and improved marine predator algorithm(IMPA) [40].

Table 1
Nomenclature and symbols.

(ι)	Scale factor	v_r	wind rated speed
$\varkappa$	Shape factor	v_{in}	Cut-in speed
v_{out}	Cut-out speed	P_{wr}	Wind rated output
ϵ	Average deviation	$G_{n(pq)}$	Transfer conductance
I_c	Critical irradiance point	ϕ_{pq}	Voltage angle between $p\&q$
I_{st}	Standard SI	lth	Load bus Voltage
λ	Weight factor	P_{Lc}	Real power of the c^{th} node
φ_{cd}	Admittance angle	I_{LF}	Inductive current
I_{Cn}	Capacitive current	α	Thyristor firing angle
P_{Gc}	Real power generation	Q_{Gc}	Reactive power generation
g_{cd}	Real part of admittance	h_{cd}	Imaginary part of admittance
$T_b^{\min}$	Bottom tap setting of transformer	$T_b^{\max}$	Upper tap setting of transformer
Q_{Cb}^{min}	Minimum VAR injection	Q_{Cb}^{max}	Maximum VAR injection
N_{sc}	Number of shunt compensator	μ	Penalty factor
N_{BL}	Number of load buses	N_T	Number of transmission line
$S_{Lb}{}^{min}$	Minimum apparent limits of power	$S_{Lb}{}^{min}$	Maximum apparent limits of power
FTV	Fittest trial vector	C	Declining coefficient
OBL	Oppositional based learning	$Mx.Ge$	Maximum generation
$P.Ge$	Present generation	CBL	Chaotis based learning
P_{sr}	Rated power of solar	$P_{D,i}$	Power demand
RESs	Renewable energy sources	PDF	Probability distribution function
TSC	Thyristor switched capacitor	TCR	Thyristor controlled reactor
ORPD	Optimal reactive power dispatch	AVD	Aggregated voltage deviation
WS	Wind speed	SI	Solar irradiance
CO	Chaotic-oppositional	r	Random variable
MMKE	Multi-trial vector-based monkey king evolution	OFs	Objective functions
k	Parts of total generation	N_{ec}	Total amount of scenarios
N_B	Load connected bus	$\overline{M}$	Evolved vector of the monkeys

Furthermore, the following algorithms have been employed: multi-objective evolutionary algorithm and integrated decision making algorithm [41], differential evolution (DE) [42], self-balanced DE (SBDE) [43], adaptive genetic algorithm [44], and simple genetic algorithm [45]. The physics-based solutions for ORPD include the harmony search algorithm [46], enhanced sine cosine algorithm [47], bio-geographic optimization algorithm [48], and gravity search algorithm (GSA) [49]. The key reasons pays behind the success of these approaches is that, these do not require continuous and differentiable functions for the objective and restrictions, they have been successful in solving the ORPD issue.

The study includes 21 different cases across three test frameworks, based on the choice of OFs, test setups, and kind of load requirement. In the first test framework, experiments were carried out in a fixed load setting without taking RESs into consideration. The latter three cases in this part utilize TSC-TCR, while the first three cases do not. The same strategy has been used in the second test framework, with the first three cases not utilizing TSC-TCR and the last three cases including TSC-TCR. In the third test framework, IEEE 118 bus is taken into account and its conventional structure has also been modified by introducing TSC-TCR & RESs. Unlike the first part, the second part adds RESs along with the test configuration, and tests are run in a variety of load environments. To represent the uncertainty of the RESs and changing load patterns, best matched PDFs have been used. Furthermore, testing are conducted in the second test framework across 25 plausible situations that are generated using MCS and BRA. The purpose of the scenario creation process is to make the scenarios closely resemble actual power network incidents.

To attain the objectives in the current ORPD study, the MMKE algorithm, which was given by Mohammad *et.al*. [50], has been used. The MMKE algorithm was developed by incorporating multi-evolutionary techniques into the monkey king evolution (MKE) [51] algorithm. MKE was inspired by a narrative from Chinese mythology, one of the algorithms in the evolution-based category. The MKE algorithm performs poorly when faced with a variety of difficulties since it only has one search strategy to handle different types of situations. However, MMKE has solved the drawbacks of its forerunner because it combines several strategies with MKE. In literature, MMKE has been successfully applied to solve the optimal power flow problem [50]. Additionally, OBL [52] & CBL [53] have been combined with MMKE and is called as COMMKE in order to accelerate the algorithm's rate of convergence. COMMKE has been employed in the current work to competently explore the search region and prevent becoming stuck on local solutions.

COMMKE outperforms other recent optimization algorithms in terms of obtaining ORPD solutions, according to testing on the various test setups stated above and a comparison of the outcomes with those stated in the literature on the iden]tical experimental framework. According to recent findings, the application of TSC-TCR also boosts system performance. Nomenclature has been included in Table 1 in the introduction section to define symbols and abbreviated terms used in the proposed research work. Results coming from COMMKE and other contemporary optimization techniques are compared using different types of statistical measurements like: providing box plots, error-bar plots, ANOVA test results etc.

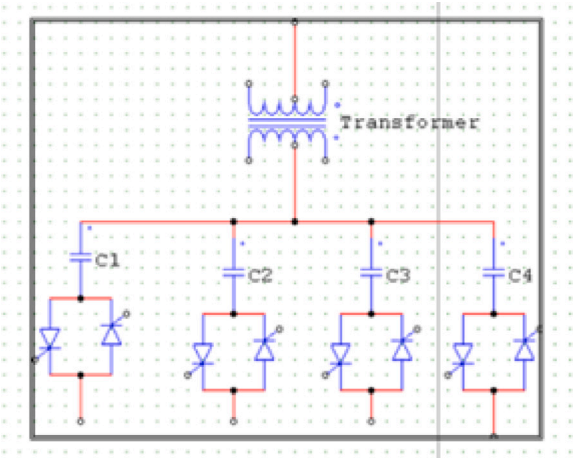

Fig. 1. Thyristor-switched capacitor (TSC).

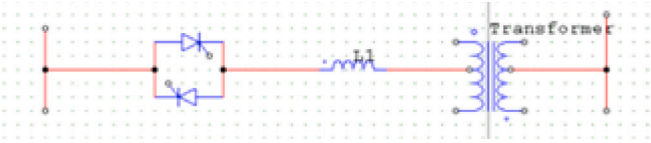

Fig. 2. Thyristor-controlled reactor (TCR).

2. Model: TSC-TCR and RESs

2.1. Modeling of TSC-TCR

2.1.1. Modeling of TSC

The thyristor-switched capacitor (TSC) kind of static compensation is depicted in Fig. 1. Bidirectional thyristor switches are used to individually turn on and off each of the distinct stages that make up the shunt-capacitor bank [54]. Through the thyristors' suppression of the gate trigger pulses, the capacitor is replaced.

2.1.2. Modeling of TCR

One of the key components of a thyristor-based static VAR compensator is a TCR. While it can function independently, it is typically utilized in tandem with fixed or thyristor-switched capacitors to offer quick, continuous reactive power regulation across the whole chosen lagging-to-leading range. TCR type of static compensation is depicted in Fig. 2.

2.1.3. Modeling of TSC-TCR

Combining TSC with TCR results in good reactive power compensation, as seen in Fig. 3. The entire reactive power in the thyristor switched capacitor scheme is divided among several parallel capacitor banks. The compensator's reactive power varies step wise in response to changes in the load or terminal voltage. A thyristor-controlled reactor and thyristor-switched capacitor banks can be used to produce a continuously changeable reactive power. The TSC-TCR combo produces a continual change in the control order from entirely lagging to fully leading current. The switched-capacitor banks and the controlled reactor operate in perfect harmony. The simple mathematical representation of net reactive power injection Q in terms of inductive current I_{LF}, capacitive current I_{Cn}, bus voltage (V) & thyristor firing angle (α) is given by:

$$Q = V \times \left[I_{LF}(\alpha_1) - \sum I_{Cn}(\alpha_2) \right] \tag{1}$$

2.2. WP model

Weibull PDF [55,56], uses parameters scale factor (ι) and shape factor ($\varkappa$)to generate a fair sketch of the variation in WS (v m/s) as:

$$f(\upsilon) = \left(\frac{\varkappa}{\iota}\right) \times \left(\frac{\upsilon}{\iota}\right)^{\varkappa-1} \times \left(e^{-\left(\frac{\upsilon}{\iota}\right)^{\varkappa}}\right) \qquad 0 < \upsilon < \infty \tag{2}$$

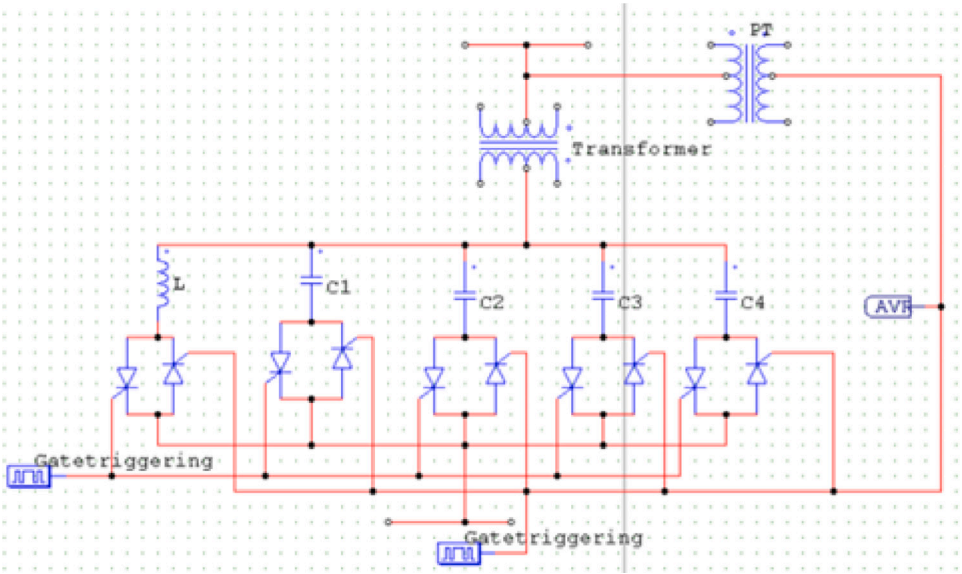

Fig. 3. Combination of TSC-TCR.

Eq. (3) represents the power output of a WT where v_r, v_{in}, v_{out} and P_{wr} denotes rated speed, cut-in speed, cut-out speed and rated output respectively.

$$P_w(v) = \begin{cases} 0 & for\ v < v_{in}\ \&\ v > v_{out} \\ P_{wr}\left(\frac{v - v_{in}}{v_r - v_{in}}\right) & for\ v_{in} \le v \le v_r \\ P_{wr} & for\ v_r < v \le v_{out} \end{cases} \tag{3}$$

Currently, the potential of WP in various WS zones may be ascertained via:

$$f(P_w)_{|P_w=0} = 1 - \exp\left[-\left(\frac{v_{in}}{\iota}\right)^{\varkappa}\right] + \exp\left[-\left(\frac{v_{out}}{\iota}\right)^{\varkappa}\right] \tag{4}$$

$$f(P_w)_{|P_w=P_{wr}} = \exp\left[-\left(\frac{v_r}{\iota}\right)^{\varkappa}\right] - \exp\left[-\left(\frac{v_{out}}{\iota}\right)^{\varkappa}\right] \tag{5}$$

$$f(P_w)_{|0<P_w<P_{wr}} = \left[\frac{\varkappa \times (v_r - v_{in})}{\iota^{\varkappa} \times P_{wr}}\right] \times \left[v_{in} + \left(\frac{P_w}{P_{wr}}\right)(v_r - v_{in})\right]^{\varkappa - 1} \times \exp\left[-\left(\frac{v_{in} + \left(\frac{P_w}{P_{wr}}\right) \times (v_r - v_{in})}{\iota}\right)^{\varkappa}\right] \tag{6}$$

2.3. PV model

It is observed that in addition to various ecological factors, the SI level affects power output of solar cell. It is also noted that the probability distribution of SI is best suited by lognormal PDF L(I) [55,57], which may be depicted as:

$$L(I) = \frac{1}{I\lambda\sqrt{2\pi}} \exp\left(\frac{-(\ln I - \epsilon)^2}{2\lambda^2}\right) \quad , \quad I > 0 \tag{7}$$

$\epsilon \& \lambda$, corresponds to the average and standard deviation of the I distribution.

The following equation illustrates how SI and a PV unit's electrical output power are related:

$$P(I) = \begin{cases} P_{nm}\frac{I^2}{I_{st}I_c}, & for\ 0 < I < I_c \\ P_{nm}\frac{I}{I_{st}}, & for\ I \ge I_c \end{cases} \tag{8}$$

P_{nm}, I_c and I_{st} respectively define the nominal output power of a PV unit, critical irradiance point, and standard SI.

3. Problem description

3.1. Fitness evaluation

The reduction of (a) APL and (b) AVD are two examples of the formation of single objectives [40] . The goals listed above are expressed as follows:

3.1.1. APL

Because of inherent resistance, APL occurs in transmission lines. The APL that must be kept to a minimum is shown as follows:

$$MinF_1 = \sum_{n=1}^{N_L} G_{n(pq)} \left(V_p^2 + V_q^2 - 2V_pV_q \cos \varphi_{pq} \right) \tag{9}$$

With a transfer conductance of $G_{n(pq)}$, the nth line joins buses $p\&q$. There are N_L transmission lines in aggregate. The voltage angle between buses $p\&q$ is ϕ_{pq}.

3.1.2. AVD

The load buses' AVD should be kept as low as possible to preserve a good voltage profile. AVD is calculated as follows:

$$MinF_2 = \sum_{l=1}^{N_B} |V_l - 1| \tag{10}$$

V_l : lth load bus Voltage; N_B: Count of load connected bus.

3.1.3. Multiple objective scenario

Employing the linear combination of APL & AVD [39], a multi-objective function has been developed as:

$$MinF_3 = APL + \lambda.(AVD) \tag{11}$$

where $\lambda(= 10)$, is identified as the weight factor.

3.2. Constraints

The following constraints apply to the ORPD problems:

3.3. Equality constraints

The following is a power flow Eq. (12) that represents the Constraint:

$$\begin{cases} \sum_{c=1}^{N_s} \left(P_{Gc} - P_{Lc} \right) = \sum_{c=1}^{N_s} \sum_{d=1}^{N_s} V_c V_d \left(g_{cd} \cos \varphi_{cd} - h_{cd} \sin \varphi_{cd} \right) \\ \sum_{c=1}^{N_s} \left(Q_{Gc} - Q_{Lc} \right) = - \sum_{c=1}^{N_s} \sum_{d=1}^{N_s} V_c V_d \left(g_{cd} \sin \varphi_{cd} - h_{cd} \cos \varphi_{cd} \right) \end{cases} \tag{12}$$

where $P_{Lc}\&Q_{Lc}$ denote the real and complex (*i.e.* reactive) power need for cth node; $P_{Gc}\&Q_{Gc}$ indicate the real and complex power of production, respectively, of the cth bus; $g_{cd}\&h_{cd}$ present respectively, the real and imaginary part the admittance of the specific line (*i.e.* $Line_{c-d}$); φ_{cd} denotes admittance angle of the specified line (*i.e.* $Line_{c-d}$)

3.4. Other constraints

(i) Restrictions for Generator:

$$\begin{cases} V_{Gb}^{\min} \le V_{Gb} \le V_{Gb}^{\max} \\ P_{Gb}^{\min} \le P_{Gb} \le P_{Gb}^{\max} \qquad b \in N_P \\ Q_{Gb}^{\min} \le Q_{Gb} \le Q_{Gb}^{\max} \end{cases} \tag{13}$$

(ii) Load bus constraints:

$$V_{Lb}^{\min} \le V_{Lb} \le V_{Lb}^{\max} \quad b \in N_{BL} \tag{14}$$

(iii) Transmission line constraints:

$$S_{Lb} \le S_{Lb}^{\max} \quad b \in N_{LT} \tag{15}$$

(iv) Transformer tap constraints:

$$T_b^{\min} \le T_b \le T_b^{\max} \quad b \in N_T \tag{16}$$

(v) Shunt compensator constraints:

$$Q_{Cb}^{\min} \le Q_{Cb} \le Q_{Cb}^{\max} \quad b \in N_{sc} \tag{17}$$

where $V_{Gb}^{min}, V_{Gb}^{max}$ present, respectively, bottom and top voltage limits, for the bth generator bus; P_{Gb}^{min}, P_{Gb}^{max} are the min and max value of active power production, respectively, of the bth bus; $Q_{Gb}^{min}, Q_{Gb}^{max}$ are the respective bottom and top reactive power production margins of the bth bus; $V_{Lb}^{min}, V_{Lb}^{max}$ voltage ranges, for the bth node; ${S_{Lb}}^{min}, S_{Lb}^{max}$ are the least and extreme apparent limits of power flow, respectively, of the bth branch; T_b^{min}, T_b^{max} present the bottom and top tap setting edges, respectively, of the bth regulating transformer; $Q_{Cb}^{min}, Q_{Cb}^{max}$ are the two extreme edges of VAR injection; N_P, N_{BL}, N_{LT}, N_T, N_{sc} denote number of generating bus; load buses; transmission line; regulating transformers and shunt compensator.

4. Optimization algorithm

4.1. MMKE algorithm

The MMKE technique consists of these vital steps: (i) Initialization, (ii) Winning-based strategy (WBS), (iii) Formation of multiple trial vector, (iv) population amendment strategy (PAS) & clustering [50].

1. **Initialization**
   Initial population size of N monkey selected within the boundary value randomly

$$H_{ij} = H_{ij}^{\min} + r * \left(H_{ij}^{\max} - H_{ij}^{\min} \right) \quad \text{for } i = 1 \, to \, N \ \& \ j = 1 \ to \ m \tag{18}$$

   where the limiting values of the jth component of the ith solution (monkey) are $H_{ij}^{\max}$ and $H_{ij}^{\min}$; The random variable r, $0 \le r \le 1$. The extents of the assessed optimization problem are m, and the positions of the N monkeys are take in the Matrix $H_{N\times m}$. $f(H_i(t))$ defines fitness evaluation at t^{th} iterative cycle.
2. **Winning-based strategy (WBS)**
   The complete generation is broken into k parts. Past generations are substituted by the fittest trial vector (FTV) with sig improvement for each segment. The improved rate IR_{Z-FTV} for each FTV is computed as follows:

$$IR_{Z-FTV} = \frac{\text{improved solutions}}{\text{function evolutions}} \tag{19}$$

   Once better rates for every FTV have been determined, the size of each FTV's sub-population is reevaluated for the upcoming n evaluation by the reward rule allocation technique. The following are the results:

$$N_{Z-FTV} = \begin{cases} 2 \times \gamma \times N & \text{because FTV is improving faster rate} \\ \gamma \times N & \text{for different FTVs} \end{cases} \tag{20}$$

   N denotes the number of monkeys, N_{Z-FTV} denotes the size of the subpopulation based on the enhanced rate of FTV, and $\gamma = 0.25$ [50].
3. **Multi-trial vector producing of MMKE**
   In the iterative process, each monkey updates its position using (a) Trial based monkey king evaluation (TBMKE), (b) Best historical trial vector evaluation (BHTVE), and (c) random based trial vector evaluation (RBTVE). The TBMKE encourages the possibility of exploration by enabling individuals to look for novel concepts in their neighborhood. With BHTVE, the regional optimum may be exploited and avoided. TVP alters its intelligent subpopulation, whereas RBTVE aims to strike a balance between exploitation and exploration. The evolved vector of the monkeys is created using the $M \& \overline{M}$ in (21). $\overline{M}$ is the binary inverse of M, which is a lower triangular matrix with all of its members set to one.

$$\begin{aligned} O_i^{M\,pop}(t+1) &= M_i \times H_i^{M\,pop} + \overline{M_i} \times V_i^{M\,pop} \\ O_i^{B\,pop}(t+1) &= M_i \times H_i^{B\,pop} + \overline{M_i} \times V_i^{B\,pop} \\ O_i^{R\,pop}(t+1) &= M_i \times H_i^{R\,pop} + \overline{M_i} \times V_i^{R\,pop} \end{aligned} \tag{21}$$

   In which $O_i^{M\,pop}, O_i^{B\,pop}$ & are the developed candidate solution for $H_i^{M\,pop}, H_i^{B\,pop}$ & $H_i^{R\,pop}$ (*i.e.* for ith monkey) within sub-populations TBMKE, BHTVE, and RBTVE is indicated by & $O_i^{R\,pop}$; the mutated vectors for i^{th} monkey are $V_i^{M\,pop}, V_i^{B\,pop} \& V_i^{R\,pop}$, representing TBMKE, BHTVE, and RBTVE, respectively.

   - **Trial based monkey king evaluation (TBMKE)**
     The fittest monkey in individual iteration is preserved as gbest from H and is kept in $gbest^{pop}$. Any monkey H_i in sub-population $H^{M\,pop}$ can be further shifted using a coefficient of fluctuation ($FC = 0.7$); two randomly selected monkeys are $H_{r1}^{M\,pop} \& H_{r2}^{M\,pop}$. A mutated vector for ith monkey of $H^{M\,pop}$ is constructed using TBMKE based on that $V_i^{M\,pop}$. It looks like this:

$$V_i^{M\,pop}(t+1) = gbest^{pop}(t) + FC \times \left(H_{r1}^{M\,pop}(t) - H_{r2}^{M\,pop}(t) \right) \tag{22}$$

Because of its extra inquisitive character in the early development and its shift to unnecessary exploitative behavior in the later optimization stages, this method will produce generally agreed-upon responses about the best monkey.

- **Best-historical trial vector evaluation (BHTVE)**
  Compared to the TBMKE, this tactic is less avaricious. By avoiding local optima catching and early convergence, it closes a lack in TBMKE. This strategy does not account for unique global best monkey, but rather for M recent finest monkeys that are maintained in the best-history archive (BHA). Within sub-population H^{Bpop}, the mutated vector V_i^{Bpop} for ith monkeys in BTVP is constructed as follows:

$$V_i^{Bpop}(t+1) = H_i^{Bhpop}(t) + C \times \left(H_{r1}^{Bpop}(t) - H_{r2}^{Bpop}(t) \right) \tag{23}$$

  A pair of randomly selected monkeys from the sub-population H^{Bpop} are H_{r1}^{Bpop} and H_{r2}^{Bpop}. C, or the declining coefficient, is given by

$$C = \xi - (\xi - \rho) \times \left(\frac{(Mx.Ge - P.Ge)}{Mx.Ge} \right)^{\mu} \tag{24}$$

  Where, $Mx.Ge$: maximum generation & $P.Ge$: present generation; $\xi = 0.001,\ \rho = 2$ [50] and $\mu = \log m$.

- **Random based trial vector evaluation (RBTVP)**
  RBTVE strikes a balance between discovery and use. The V_i^{Rpop} mutated vector in RBTRE is produced as follows for ith monkeys of sub-population H^{Rpop}:

$$\begin{aligned} V_i^{Rpop}(t+1) = {} & H_i^{Rpop}(t) + F_i \times \left(H_{r1}^{Rpop}(t) - H_i^{Rpop}(t) \right) \\ & + F_i \times \left(H_{r2}^{Rpop}(t) - H_j^{Alpop}(t) \right) \end{aligned} \tag{25}$$

  among sub-populations H_i^{Rpop}, H^{Rpop} is monkey ith, whereas H_{r1}^{Rpop} and H_{r2}^{Rpop} are respectively $r1$th and $r2$th monkeys at random; H_j^{Alpop} Any random monkey in $H \bigcup H^{Bhpop}$ is; scale factor F_i is a number between 0 and 1 [58].

4. **Population amendment strategy (PAS)**
   One generation of monkeys grows, and the fitness of the offspring is assessed and compared to that of the progenitor monkeys. The succeeding generation is composed of just the most successful monkeys.
5. **Clustering**
   When low-quality monkeys are seen, they are kept so they can share their expertise with the monkeys of the future in order to achieve a broad range of basic and compound challenges. This might prevent the search from taking place in areas that are not fruitful or close to inferior monkeys. N is the maximum number of monkeys that the repository can hold. When it surpasses N, the monkey with the longer lifespan is expelled.

4.2. OBL

OBL [59] has been integrated with conventional MMKE in order to locate the search space for the best solution more efficiently and to speed up the search process. Tizhoosh developed the OBL, a demanding optimization method [52]. It promotes increasing convergence and raising the correctness of the answer. The starting population for basic MMKE is produced randomly inside a designated search space using (18).

Initially, the MMKE started with a randomly generated population. This adds time to the process of finding the global best solution. In a local solution, there could also be chances for speedy trapping. By integrating OBL with basic MMKE, these problems are avoided. The OBL scheme's opposing amount resides in the candidate solution's mirror spot. In OBL, a previously randomly generated population is used to construct the opposing population (OP) in the manner described below:

$$OP_{H\,ij} = H_{ij}^{\min} + H_{ij}^{\max} - H_{ij} \quad \text{for } i = 1\ to\ N\ \&\ j = 1\ to\ m \tag{26}$$

Based on the jump rate, this OBL concept is used at beginning and during each iteration. The following are the steps involved in OBL:

Step 1: Determine the associated fitness values after randomly generating a population H under the operation's limit.
Step 2: Build OP by using (26)
Step 3: Evaluate the fitness value of OP.
Step 4: Put the current population and the OP in order of best to worst.
Step 5: With respect to the population size N, pick N numbers of the best solutions from both the present population and the OP.
Step 6: Revise the provided problem's parameters using the recommended optimization method.
Step 7: Based on the hopping rate, OP is created from the current population. [60].
Step 8: In order to choose the N fittest solution for the subsequent iteration, assemble the current population & OP from best to worst.
Step 9: Proceed to step 6 for the subsequent iteration or terminate the loop based on the stopping criteria.

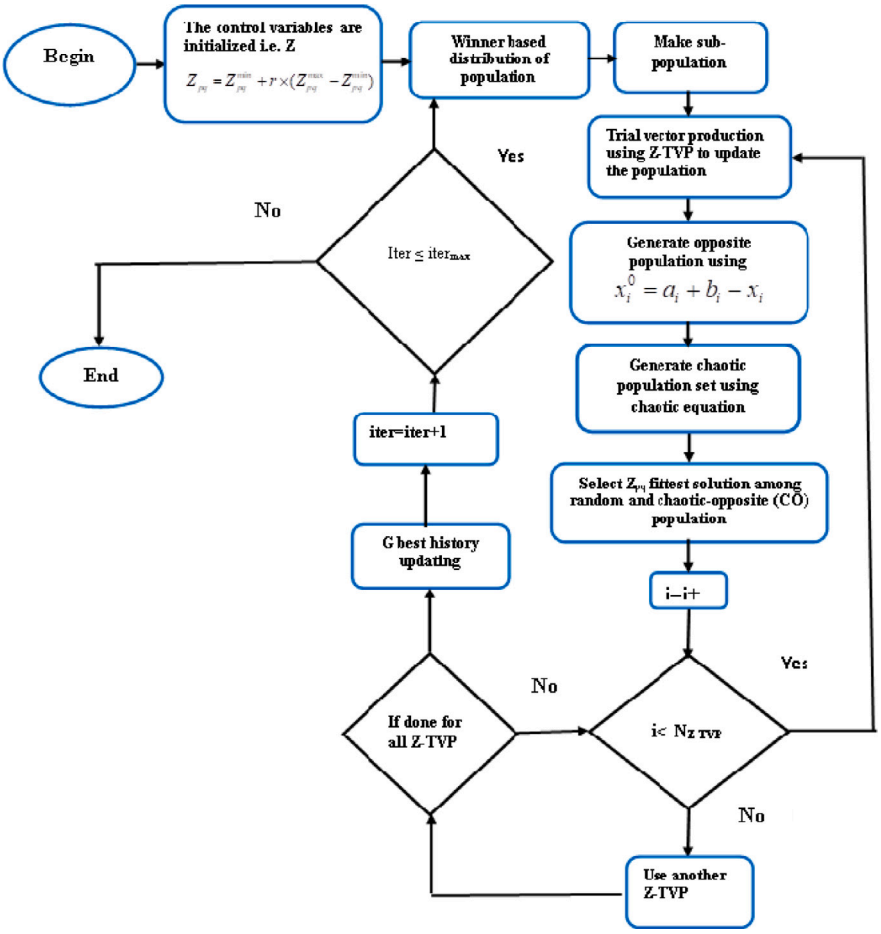

Fig. 4. Flowchart of COMMKE.

4.3. Chaotic based learning (CBL)

Most evolutionary algorithms learn from the population's random initialization and continuous search for the optimal solution. In finding the global optimal solution, which also affects the pace of convergence, MMKE is still not able to beat other techniques. To mitigate this impact, the MMKE is combined with chaotic behavior to generate the COMMKE. The non-repeating and unexpected characteristics of chaos enable speedier searches in general, which might be important for quickening the convergence of a metaheuristic algorithm.

Several chaotic maps are merged with MMKE in the COMMKE approach to regulate the parameters of MMKE. Ten chaotic maps exhibiting distinct behaviors comprise the chaotic set combination. In the range of 0 to 1, the starting value for the ideal solution is 0.7. Table 2 discusses the different chaotic maps. With the use of these chaotic maps, the local optimal issue has been solved, yielding the global optimal solution.

Various chaotic maps are taken into consideration in the COMMKE optimization problem in order to manage the MMKE's parameters. Ten distinct chaotic maps with varying behaviors are selected for the chaotic set. This set's starting point is located at 0.7 in the interval between 0 and 1. The distinct characteristics of chaotic maps aid in the resolution of local optima and convergence speed issues.

Fig. 4 shows the flowchart of the suggested COMMKE optimization approach.

4.4. Drawbacks of COMMKE algorithm

The drawbacks of the COMMKE algorithm are discussed as follows:

1. **Parameter Sensitivity**: As performance is heavily depended on the choice of control parameters, poor parameter tuning can lead to stagnation or premature convergence.
2. **Premature convergence** Still converge prematurely, especially in deceptive or high-dimensional multimodal functions.

Table 2
List of different chaotic maps.

Sl. No.	Name	Chaotic map
N1	Circle	$r_{k+1} = r_{k+b} - (a/2\pi)sin(2\pi k)\, mod\ (2)$
N2	Cubic	$r_{j+1} = ar_j\left(1 - r_j^{\,2}\right)$
N3	Chebyshev map	$r_{j+1} = \cos\left(k\cos^{-1}\left(r_k\right)\right)$
N4	Logistic map	$r_{k+1} = ar_k\left(1 - r_k\right)$
N5	Gussian map	$r_{k+1} = r_{k+1}\left\{0\ ,\ r_k = 0\ ,\ \frac{1}{r_k}\ \mathrm{mod}\ \ (1) = \frac{1}{r_k} - \left[\frac{1}{r_k}\right]\right.$
N6	Liebovitch map	$r_{k+1} = ar_k\left(1 - r_k\right)$
N7	Iterative map	$\mathrm{r_{k+1}} = \mathrm{Sin}\left(\frac{\mathrm{a}\,\pi}{\mathrm{ik}}\right), \alpha \in (\mathrm{U},1)$
N8	Sine	$X_{i+1} = a/4\left(sin\prod x\right)$
N9	Sinusoidal	$X_{i+1} = a\left(X_i\right)2\left(sin\prod x_i\right)$
N10	Tent	$X_{i+1} = \begin{cases} \frac{X_i}{0.7}; & \mathrm{X}_i < 0.7 \\ \frac{10}{3}(1 - X_i)\ ; & \mathrm{X}_i \geq 0.7 \end{cases}$

Table 3
An overview of IEEE 30-bus System.

Items	Base configuration		Adapted configuration	
	Quantity	Details	Quantity	Details
Buses	30	[39]	30	[39]
Branches	41	[39]	41	[39]
Thermal generators	6	Buses:1 (swing), 2, 5, 8, 11, and 13	4	$T_1(swing), T_2,\ T_{11,}$and T_{13}
Wind generators	–	–	2	W_5
Solar PV unit	–	–	1	Bus: PV_8
Transformer	4	$L_{6-9},\ L_{6-10},\ L_{4-12},$ andL_{25-27}	4	$L_{6-9},\ L_{6-10},\ L_{4-12},$ andL_{25-27}
Control variables	19	V_G: (6Nos.) Transformer: 4 and VAR injection: 9	19	V_G: 6 4 and VAR injection: 9
Load demand	–	283.4MW, 126.2MVAr	–	Variable
Range of load bus voltage	24	[0.95–1.05]p.u.	24	[0.95–1.05]p.u.
TSC-TCR	–	–	1	Result obtained using COMMKE
Compensation devices	9	$VAR_{10},\ VAR_{12},\ VAR_{15},\ VAR_{17},\ VAR_{20},$ $VAR_{21}, VAR_{23}, VAR_{24}, VAR_{29}$	9	$VAR_{10},\ VAR_{12},\ VAR_{15},\ VAR_{17},\ VAR_{20},$ $VAR_{10},\ VAR_{12},\ VAR_{15},\ VAR_{17},\ VAR_{20}$

Table 4
Specifics of the PDFs used for RESs.

Specifications	WG (bus 45)	PV (bus 16)
PDF	Weibull	Lognormal
Rated power (MW)	80	80
Parameters	$\xi = 10, \kappa = 2$	$\epsilon = 6, \lambda = 0.6$

3. **Hyperparameter Explosion**: Adding chaos and opposition concept increases the number of parameters to be tuned, this can make the algorithm harder to configure and deploy.

5. Simulation outcomes and comparisons

This section presents the simulation findings for a number of ORPD investigations using the COMMKE approach and compares them with earlier studies [39]. The complete simulations is done using the MATLAB platform. Convectional and modified architectures of the IEEE 30-bus network have been chosen as test systems. Table 3 offers a succinct synopsis of test system configurations, with one being the base configuration and the other being an adjusted configuration.

This study may be roughly split into two test frameworks based on the different test setting types. To enable fair comparison, the test systems are selected based on the same system as that used in [39]. In test framework one, only thermal generators are considered; in test framework two, RESs are introduced with the conventional generators. For WS and SI fluctuations, the PDF (respectively, Weibull & Lognormal based) details are shown in Table 4 and depicted in Fig. 5.

These two test networks are used to examine a total of 12 cases, which are collected in Table 5. Test framework one looks at cases 1–6, whereas Test framework two looks at cases 7–12. One can further subdivide test frameworks 1 and 2 into two sections: the first does not employ TSC-TCR, while the second uses TSC-TCR as an integrated FACTs tool inside the test network. Particularly, for cases 1–3 and 7–9, TSC-TCR is not considered; in contrast, cases 4–6 and cases 10–12 are examined while TSC-TCR is being used with the test network. With the exception of swing generators, the active power settings for generators in the context of optimization need to be carefully selected while staying within the generators' specified limits. Table 6 (as an appendix) displays these quantities for cases 1–6 and cases 7–12 during the inquiry. For every test setup, three objectives are met. They are decrease in APL and reduction in AVD as single objectives and concurrently decreasing APL & AVD as multi-objective cases.

Table 5
Several case studies.

Case	objective		Fitness function	Constraints	IEEE system
	Single	Multiple			
1	✓		APL minimization	Equality	
2	✓		AVD minimization	and	30 Bus
3		✓	Simultaneous minimization of APL and AVD	inequality	
4	✓		APL minimization	Equality	30 Bus
5	✓		AVD minimization	and	with
6		✓	Simultaneous minimization of APL and AVD	inequality	TSC-TCR
7	✓		APL minimization	Equality	30-Bus with
8	✓		AVD minimization	and	solar
9			Simultaneous minimization of APL and AVD	inequality	& wind
10	✓		APL minimization	Equality	30-Bus with solar-wind
11	✓		AVD minimization	and	and TSC-TCR
12		✓	Simultaneous minimization of APL and AVD	inequality	
13	✓		APL minimization	Equality	
14	✓		AVD minimization	and	118 Bus
15		✓	Simultaneous minimization of APL and AVD	inequality	
16	✓		APL minimization	Equality	118 Bus with
17	✓		AVD minimization	and	TSC-TCR
18		✓	Simultaneous minimization of APL and AVD	inequality	
19	✓		APL minimization	Equality and	118-Bus with
20	✓		AVD minimization	inequality	solar-wind and
21		✓	Simultaneous minimization of APL and AVD		TSC-TCR

Table 6
Appendix: IEEE 30 bus system's generator data.

Type	Bus	Pg		Qg		Cases 1-6	Cases 7-12
	no.	min	max	min	max		
	1	50	200	−20	150	Swing	Swing
Thermal	2	20	80	−20	60	75	75
	5	15	50	−15	62.5	40	40
Wind	5	0	75	−30	35		Variable
Solar	8	0	50	−20	25		Variable
	8	10	35	−15	48.7	30	30
Thermal	11	10	30	−10	40	25	25
	13	12	40	−15	44.7	30	30

5.1. Test framework one

The test network for this framework is included in Table 3, under the "Base configuration" section. This test configuration is used for cases 1–6. TSC-TCR is linked with the test network for cases 4–6. In this part, the experiments have been carried out with a network loading (constant) of 100 Here are the computed results for cases 1–3 and cases 4–6, respectively, shown in Tables 7 and 8. Along with variable's optimal and boundary values, these tables show the computed magnitudes of the objective quantities. In contrast to COMMKE in present study, the success history-based adaptive differential evolution (SHADE) algorithm was used in [39], where a comparable test setup was implemented.

Table 7 shows that, in case-1, APL is computed as 4.3001(MW) using COMMKE, which is less than 0.1125 (MW) when compared to the results in [39]. As determined by COMMKE, the AVD in case-2 is 0.08858 p.u., which is less than the 0.00028 p.u. derived from the results reported in [39]. When simultaneous objectives are considered in case 3, the results are appreciably improved. The computation time for every case in the final row is included in these results. Compared to [39], it has been noted that using COMMKE not only leads to better optimization for cases 1–2 but also accomplishes the objective of obtaining better outcomes in a shorter amount of time. Table 8 gives the results of the experiments conducted while taking TSC-TCR on base configuration into consideration. APL of 4.3001 MW in case-1 drops to 4.2 MW in case-4, and AVD in case 2 drops by 0.00248 (p.u.) in case-5, according to the comparison of Tables 7 & 8. APL and AVD were 4.89 (MW) and 0.1297 p.u., respectively, in case 3 (*i.e.* , the system without TSC-TCR), while they are 4.84 (MW) and 0.1038 p.u., respectively, in case 6 (which has TSC-TCR attached), when the achievement of multiple objectives (in cases 3 and 6) is taken into account. APL and AVD were 4.89 (MW) and 0.1297 p.u., respectively, in case 3 (*i.e.* , the system without TSC-TCR), while they are 4.84 (MW) and 0.1038 p.u., respectively, in example 6 (which has TSC-TCR attached), when the achievement of multiple objectives (in cases 3 and 6) is taken into account. It makes quite evident how TSC-TCR can be used to enhance system performance.

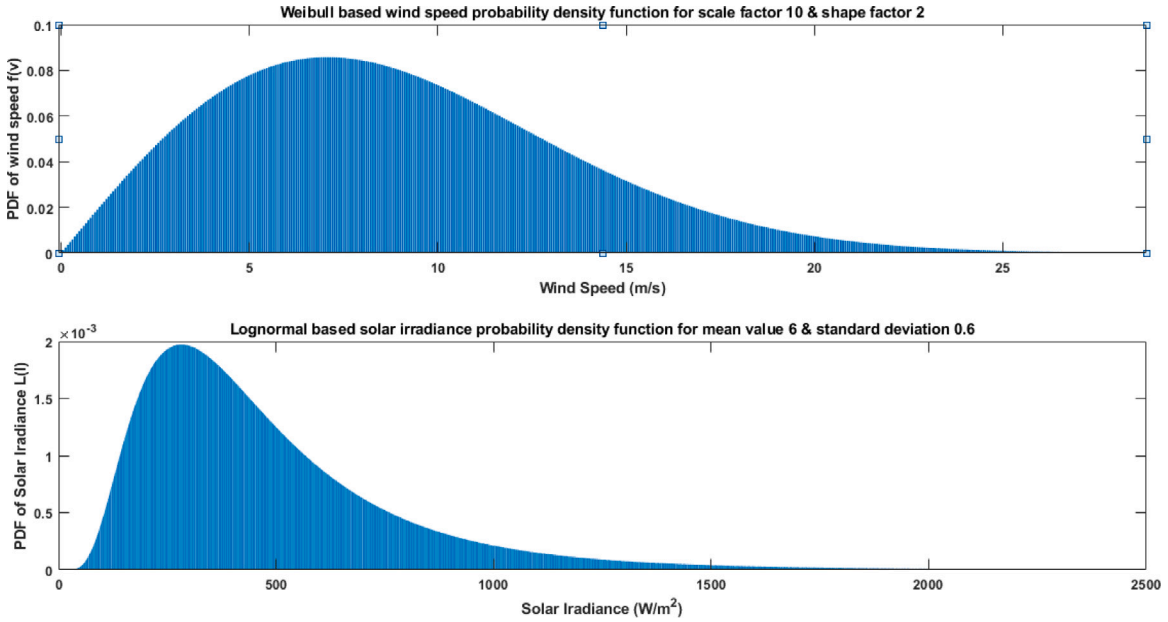

Fig. 5. Weibull based WS PDF with $\iota = 10$ and $\varkappa = 2$, Lognormal based SI (W/m^2) PDF with $\varepsilon = 6$ and $\lambda = 0.6$.

Table 7
Optimal results with rated load of 30-bus network without FACTS.

Control parameters		Min.	Max.	Case1 [39]	Case1 COMMKE	Case2 [39]	Case2 COMMKE	Case3 COMMKE
Generators' Voltage (p.u.	V1	0.95	1.1	1.0694	1.0771	1.0045	1.0099	1.0479
	V2			1.0609	1.0678	1.0019	1.0069	1.0333
	V5			1.0375	1.0425	1.0203	1.0207	1.0088
	V8			1.0434	1.045	1.0063	0.9993	1.0006
	V11			1.0918	1.0965	1.0268	1.0351	1.02
	V13			1.0508	1.0914	1.0222	1.0183	1.0032
Transfor-mers' turns ratio	$Line_{11}$	0.9	1.1	1.04	1.004	1.04	1.0441	1.0336
	$Line_{12}$			0.96	0.9211	0.9	0.9046	0.9035
	$Line_{15}$			0.98	0.9801	1	0.9958	0.9923
	$Line_{36}$			0.98	0.9516	0.96	0.9583	0.9484
VAr Injection	VAR_{10}	0	5	2.8	4.68	4.6	4.99	4.39
	VAR_{12}			0.4	4.7	0.2	1.05	4.56
	VAR_{12}			0.2	4.71	5	5	4.92
	VAR_{17}			5	4.79	0.2	0.17	1.77
	VAR_{20}			4	4.22	5	5	4.91
	VAR_{21}			5	4.76	5	5	3.9
	VAR_{23}			3	2.52	5	4.99	4.87
	VAR_{24}			5	4.93	5	5	4.15
	VAR_{29}			2.6	2.39	2	1.99	0.56
APL(MW)				**4.4126**	**4.3001**	5.4495	5.28	**4.89**
AVD(p.u.)				0.9029	1.6211	**0.08886**	**0.08858**	**0.1297**
Generators' reactive power	QG1	−20	150	−0.2645	−2.19	−20	−19.94	13.38
	QG2	−20	60	15.7848	10.26	−9.8371	−6.95	11.85
	QG5	−15	62.5	24.9606	21.95	61.4656	57.72	28.97
	QG8	−15	48.7	29.1134	18.57	48.7	30.26	21.01
	QG11	−10	40	24.6734	11.93	13.7823	17.55	9.94
	QG13	−15	44.7	1.1666	5.59	10.2631	7.34	−2.93
CPU Time (s)				149.6	148.87	148.4	147.6	146.8

The convergence properties of APL minimization and AVD minimization with and without taking TSC-TCR into account are shown in Fig. 6. The curves in Fig. 6 make it evident how adding TSC-TCR (*i.e.* , FACTS devices) to the power network improves system performances. Voltage variation for cases 2 & 5 are shown in Fig. 7 over the whole load buses.

Table 8
Optimal results with rated load of 30-bus network incorporating TSC-TCR.

Control Parameters		Min.	Max.	Case 4 [COMMKE]	Case 5 [COMMKE]	Case 6 [COMMKE]
Generators' voltage (p.u.)	V1	0.95	1.1	1.0896	1.0155	1.0257
	V2			1.082	1.0119	1.0152
	V5			1.0561	1.0251	0.9965
	V8			1.0621	0.988	0.9904
	V11			1.0966	0.9932	1.058
	V13			1.0972	1.0485	0.9847
Transformers' turns ratio	$Line_{11}$	0.9	1.1	1.02	0.9961	1.0675
	$Line_{12}$			0.9237	0.9628	0.963
	$Line_{15}$			0.9998	1.0481	0.9852
	$Line_{36}$			0.9757	0.9771	0.9776
Generators' reactive power (MVAr)	VAR_{10}	0	5	4.11	2.44	2.87
	VAR_{12}			4.88	0.05	4.85
	VAR_{15}			4.03	0.95	4.29
	VAR_{17}			4.8	0.17	2.94
	VAR_{20}			3.46	4.93	4.33
	VAR_{21}			4.86	4.78	2.46
	VAR_{23}			2.81	2.04	1.89
	VAR_{24}			4.91	4.88	4.77
	VAR_{29}			2.74	0.3	3.38
Optimal location		−10	10	22	30	29
QTSC-TCR(MVAr)				6.7	9.957	8.65
APL(MW)				4.2	5.38	4.84
AVD(p.u.)				1.6876	0.0861	0.1038
Generators' reactive power (MVAr)	Q1	−20	150	−7.01	−18.48	0.11
	Q2	−20	60	11.55	−3.34	4.28
	Q5	−15	62.5	19.93	61.36	28.69
	Q8	−15	48.7	21.07	6.13	6.09
	Q11	−10	40	11.75	−2.69	30.03
	Q13	−15	44.7	9.12	29.62	−13.36
CPU Time (s)				147.32	146.87	146.11

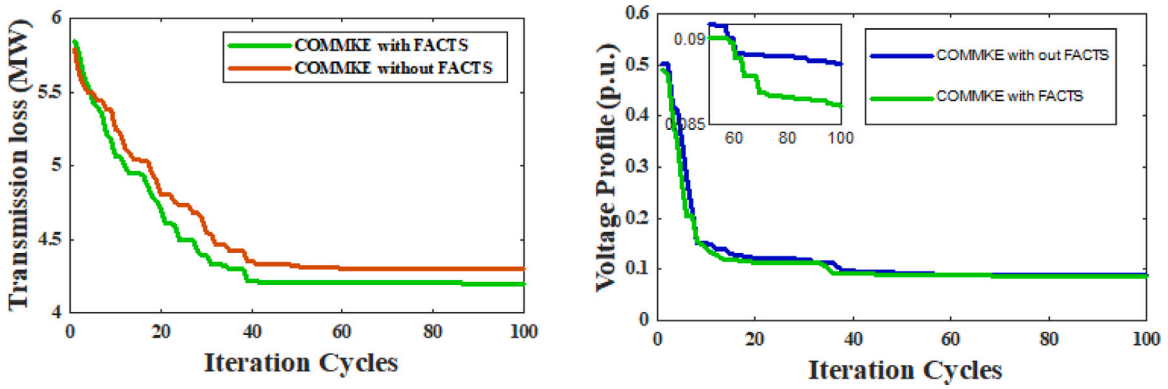

Fig. 6. Convergence characteristics of APL and AVD using COMMKE with and without TSC-TCR.

5.2. Test framework two

The right-hand side of Table 3, referred as a "adapted configuration". In this setup, conventional model is enhanced by RESs (WP and PV). As can be seen in Table 5, six cases (cases 7–12) in total are taken into consideration in this section of the experiment. Three of the cases (cases 7–9) are conducted using test setup without taking TSC-TCR into account, and the remaining cases (cases 10–12) are conducted over the test network using TSC-TCR.

5.2.1. Scenario creation & reduction

Moreover, this mode of experiment has employed the procedure of scenario construction and scenario shrinking to manage the load's unpredictable nature and the volatility of RESs [39]. For estimating unknown load demand, a normal PDF with a mean of 70 and a standard deviation of 10 has been taken into account [39]. In the process of developing scenarios, weibull and lognormal PDFs

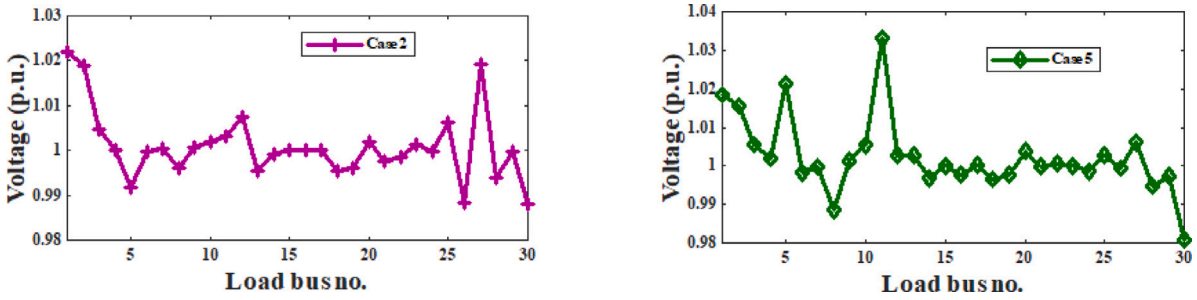

Fig. 7. Voltage deviations over load buses for case 2 & 5.

are used to describe uncertain WS and SI, respectively, with parameter values as given in Table 4. During scenario development, non-zero PV power contribution is allocated to 50% of the probability and nil irradiance is assigned to 50% of the probabilities because the sun is visible for only half of a 24-hour day. WS, SI, and load demand are included in a scenario. It is shown as:

$$S_i = [P_{D,i}, v_{w,i}, I_i] \tag{27}$$

where S_i indicates ith scenario; $P_{D,i}$ depicts power demand in ith scenario; $v_{w,i}$ indicates WS in ith scenario and I_i denotes SI in ith scenario.

First, a set of 1000 scenarios is created by combining the 1000 Monte-Carlo choices for load demand, WS & SI together. BRA has narrowed down these 1000 scenarios to 24, because it is not feasible to manage 1000 possible outcomes [61]. These 24 scenarios represent situations at 24 h of a day. Initially, N_0 scenarios with identical probabilities ($\rho_0 = \frac{1}{N_0}$) are considered. In an attempt to decrease the number of possibilities, one scenario is eliminated following each BRA iteration. The BRA's scenario reduction phases are illustrated as follows:

1. **Initialization**

   - Create N_0 distinct scenarios (S_i) for $i = 1, 2, \ldots, N_0$. As of right now, $N_0 = 1000$.
   - Every scenario starts with an equal probability of occurring ($\rho_0 = \frac{1}{N_0}$).
     Measure the distance between every pair of scenarios d_{ij}, where $d_{ij} = \left\| S_i - S_j \right\|$
   - Make a distance matrix D with d_{ij}, where diagonal components $d_{ii} = 0$ and early dimension $N_0 \times N_0$.
   - Create the running variable $N_r = N_0$ and the N_{ec} conclusion criterion, which indicate the number of final scenarios that have been chosen.

2. **Recurring events**

   Step 1: Aside from the self-distance $d_{ii} = 0$, find the smallest distance value from D. Assume that the separation between the mth and nth scenarios, d_{mn}, is at least in D. Then, take into consideration the scenarios S_m&S_n, which have respective chances of ρ_m&ρ_n.

   Step 2: Delete scenario n if $\rho_m \geq \rho_n$ & update the likelihood $\rho_m = \rho_m + \rho_n$. If not, remove scenario m. $\rho_n = \rho_m + \rho_n$ should be updated.

   Step 3: Modify $N_r = N_r - 1$.
   Evaluate the matrix D again, taking into account the separation between each pair of existing cases.

   Step 4: If $N_r > N_{ec}$, then repeat step 1 and go on.
   Else, END.

These 24 possibilities, together with the associated probabilities that result from applying BRA to 1000 initial scenarios, are shown in Table 10.

In column two of Table 10, the load demand is shown as % loading. Fig. 8 shows the hourly load demand variations, WS variations & changes in SI respectively over 24 h (a day). The WP and PV power are computed using (3) and (8), correspondingly and indicated in Table 10. The optimization method, which minimizes the combined APL & AVD as a multi-objective and the individual APL and AVD as a single goal, is now conducted independently for each scenario to extract the value of the OFs. To find the minimal APL for each scenario and so forth for other considered OFs, the optimization procedure has been performed 24 times, as there are 24 possibilities evaluated in the current study. The minimal APL (in line with case 7) & minimum AVD (in line with case 8) for each situation as listed in Table 10 are presented in Table 11. An anticipated APL (EAPL) (for case 7) and with an anticipated AVD (EAVD) (for case 8) are also shown in Table 10. These are derived from the likely calculated APL & AVD for every scenario. EAPL & EAVD are calculated as follows, respectively:

$$EAPL = \sum_{i=1}^{N_{ec}} \rho_i \times APL \tag{28}$$

Table 9
Sensitivity analysis for active power loss (APL) with variation of wind parameters.

Variation of wind parameters		Active power loss without FACTS using COMMKE			Active power loss incorporating TSC-TCR using COMMKE		
Shape factor	Scale factor	Best APL (MW)	Average APL (MW)	Worst APL (MW)	Best APL (MW)	Average APL (MW)	Worst APL (MW)
3.958	1.413	4.3452	4.3468	4.3486	4.2321	4.2349	4.2371
4.012	2.116	4.3434	4.3441	4.3472	4.2317	4.2342	4.2366
4.048	2.818	4.3416	4.3431	4.3474	4.2308	4.2335	4.2389
4.103	3.518	4.3397	4.3412	4.3466	4.2296	4.2312	4.2377
4.206	4.237	4.3382	4.3399	4.3462	4.2276	4.2342	4.2392
4.216	4.892	4.3338	4.3371	4.3416	4.2252	4.2316	4.2358
4.241	5.662	4.3313	4.3329	4.3363	4.2230	4.2251	4.2283
4.278	6.382	4.3282	4.3298	4.3316	4.2238	4.2258	4.2302
4.331	7.124	4.3241	4.3253	4.3297	4.2214	4.2236	4.2284
4.369	7.778	4.3205	4.3267	4.3306	4.2121	4.2154	4.2183
4.416	8.489	4.3001	4.3026	4.3103	4.2000	4.2046	4.2111

Table 10
Load demand, solar irradiance, wind velocity (WV) and wind power (WP), together with the corresponding probability under different scenarios.

Scenario	Demand percentage	WV (m/s)	Irradiance (W/m^2)	WP (MW)	PV power (MW)	Probability
1	60	16.5634	0	75	0	0.0417
2	60	16.4355	0	75	0	0.0417
3	70	15.9872	0	74.9262	0	0.0417
4	70	14.6734	0	67.3465	0	0.0417
5	70	13.6735	0	61.5781	0	0.0417
6	80	11.6537	85.7652	49.9252	3.0649	0.0417
7	80	10.6734	107.4453	44.2696	4.8102	0.0417
8	90	9.8736	545.8764	39.6554	27.2938	0.0417
9	90	8.6735	765.9754	32.7317	38.2988	0.0417
10	90	7.6735	898.6453	26.9625	44.9323	0.0417
11	100	7.7632	997.7382	27.48	49.8869	0.0417
12	110	6.6734	1098.6743	21.193	50	0.0417
13	110	5.7843	1201.5634	16.0633	50	0.0417
14	100	5.4531	1082.4984	14.1525	50	0.0417
15	100	4.7638	813.7609	10.1758	40.688	0.0417
16	90	3.8735	754.5645	5.0391	37.7282	0.0417
17	90	3.2343	695.8981	1.3517	34.7949	0.0417
18	100	4.6754	406.9891	9.6658	20.3495	0.0417
19	110	4.5635	145.7676	9.02	7.2884	0.0417
20	110	3.6725	0	3.8795	0	0.0417
21	110	6.5634	0	20.5581	0	0.0417
22	100	7.4523	0	25.6863	0	0.0417
23	90	9.7865	0	39.1529	0	0.0417
24	70	12.9877	0	57.6213	0	0.0417

$$EAVD = \sum_{i=1}^{N_{ec}} \rho_i \times AVD \tag{29}$$

where N_{ec} is the total amount of scenarios; ρ_i is the likelihood of ith scenarios.

The results of case 9, in which APL and AVD are simultaneously minimized for each 24 scenarios of Table 10, are shown in Table 12. Using the same test configuration with TSC-TCR and created scenarios, experiments for cases 10 through 12 are conducted. For cases 10 through 11, the experimental findings are shown in Table 13, and for case 12, the results are displayed in Table 14.

Applications of COMMKE to test systems with and without TSC-TCR have yielded the following points:

- EAPL decreases to 4.2104 MW with TSC-TCR (case 10) from 4.6441 MW without TSC-TCR (case 7).
- The EAVD (in case 8) was 0.1133 p.u. without TSC-TCR, but when TSC-TCR is incorporated (in instance 11), it decreases to 0.1048 p.u..
- In comparison to case-9 (*i.e.* , without TSC-TCR), case-12's connecting TSC-TCR lowers EAPL & EAVD by 0.4545 MW & 0.0042 p.u., respectively, while cases 9 and 12 are observed simultaneously.

This comparative research shows that performance is improved by lowering both APL and AVD when TSC-TCR is added to the power network.

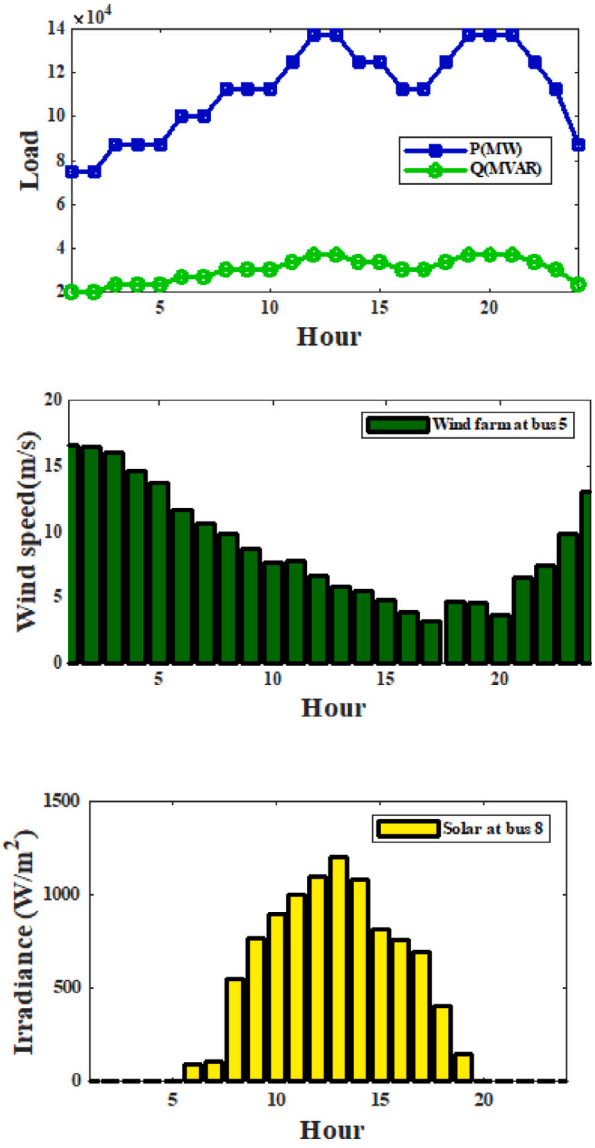

Fig. 8. Hourly load demand variations, WS variations & changes in SI respectively.

Under uncertainty scenarios 12, the voltage deviations for cases 8 and 11 at various load buses are shown in Fig. 9. In case 8, TSC-TCR is not introduced with test network where as in case 11 test set-up is considered with TSC-TCR. The improvement of the VD profile when TSC-TCR is implemented with the test systems may be investigated by closely examining Fig. 9.

In order to judge the robustness of the proposed COMMKE algorithm, sensitivity analysis on IEEE 30-bus system with and without FACTS devices for active power loss (APL) minimization has been performed and illustrated in Table 9. In this sensitivity analysis, APL variation with changing of shape factor and scale factor of the wind speed has been discussed. The sensitivity analysis clearly proves the superiority and robustness of the proposed optimization with changing the input parameters.

5.3. Test framework three

In this part of the study, the conventional IEEE 118 bus network is chosen first, where cases 13–15 are conducted. Then cases 16 to 18 are performed on the IEEE 118 bus embedded with TSC-TCR as a FACTS tool. Finally, cases 19–21 are carried on the IEEE 118 bus network considering FACTs tool and RESs (wind,solar). The descriptions of cases 13–21 are provided in Table 5. The overview of the test systems are shown in Table 15. Table 16 shows the outcomes while cases 13–18 are conducted. These cases are studied under fixed loading (100%) basis without considering time varying WP & PV power. The computed results using COMMKE are as follows:

Table 11
Simulation utilizing COMMKE (Single objective) with time-varying demand and unknown renewable power.

Scenario /Hour	Loading percentage	WP (MW)	PV power (MW)	Scenario probability	Scenario based APL (MW)	Scenario based AVD (p.u.)
1	60	75	0	0.0417	0.87	0.0754
2	60	75	0	0.0417	0.88	0.0756
3	70	74.9262	0	0.0417	1.19	0.0821
4	70	67.3465	0	0.0417	1.28	0.081
5	70	61.5781	0	0.0417	1.31	0.0732
6	80	49.9252	3.0649	0.0417	2.36	0.0982
7	80	44.2696	4.8102	0.0417	2.29	0.0879
8	90	39.6554	27.2938	0.0417	3.1	0.0988
9	90	32.7317	38.2988	0.0417	2.99	0.0975
10	90	26.9625	44.9323	0.0417	3.16	0.1001
11	100	27.48	49.8869	0.0417	4.31	0.1304
12	110	21.193	50	0.0417	6.61	0.1592
13	110	16.0633	50	0.0417	6.99	0.1584
14	100	14.1525	50	0.0417	5.15	0.1358
15	100	10.1758	40.688	0.0417	5.88	0.148
16	90	5.0391	37.7282	0.0417	4.62	0.0976
17	90	1.3517	34.7949	0.0417	5.33	0.0955
18	100	9.6658	20.3495	0.0417	7.04	0.1311
19	110	9.02	7.2884	0.0417	11.03	0.1543
20	110	3.8795	0	0.0417	11.99	0.1576
21	110	20.5581	0	0.0417	10.21	0.1598
22	100	25.6863	0	0.0417	7.17	0.1323
23	90	39.1529	0	0.0417	4.28	0.1023
24	70	57.6213	0	0.0417	1.33	0.0851
Case 7:					Case 8:	
EAPL = 4.6441 MW					EAVD = 0.1133 (p.u.)	

Table 12
Simulation utilizing COMMKE (Multi-objective) with time-varying demand and fluctuating renewable power.

Scenario	Loading percentage	WP (MW)	PV Power (MW)	Scenario probability	Fitness value (Case 9)	APL (MW)	AVD (p.u.)
1	60	75	0	0.0417	1.777	0.979	0.0798
2	60	75	0	0.0417	1.822	1.023	0.0799
3	70	74.9262	0	0.0417	2.2	1.324	0.0876
4	70	67.3465	0	0.0417	2.346	1.525	0.0821
5	70	61.5781	0	0.0417	2.418	1.673	0.0745
6	80	49.9252	3.0649	0.0417	3.757	2.761	0.0996
7	80	44.2696	4.8102	0.0417	3.597	2.699	0.0898
8	90	39.6554	27.2938	0.0417	4.817	3.652	0.1165
9	90	32.7317	38.2988	0.0417	4.628	3.452	0.1176
10	90	26.9625	44.9323	0.0417	4.774	3.587	0.1187
11	100	27.48	49.8869	0.0417	6.315	4.962	0.1353
12	110	21.193	50	0.0417	8.89	7.269	0.1621
13	110	16.0633	50	0.0417	9.364	7.746	0.1618
14	100	14.1525	50	0.0417	7.052	5.664	0.1388
15	100	10.1758	40.688	0.0417	7.943	6.432	0.1511
16	90	5.0391	37.7282	0.0417	6.28	5.268	0.1012
17	90	1.3517	34.7949	0.0417	7.015	6.023	0.0992
18	100	9.6658	20.3495	0.0417	9.162	7.797	0.1365
19	110	9.02	7.2884	0.0417	13.694	12.118	0.1576
20	110	3.8795	0	0.0417	14.598	12.987	0.1611
21	110	20.5581	0	0.0417	12.764	11.121	0.1643
22	100	25.6863	0	0.0417	9.366	8.001	0.1365
23	90	39.1529	0	0.0417	6.243	5.132	0.1111
24	70	57.6213	0	0.0417	2.637	1.761	0.0876
Case 9:				EAPL = 5.2107 MW		EAVD = 0.1189 p.u.	

1. In case 13, APL is 123.786 MW, whereas in case 16 APL is 122.453 MW. It means use of TSC-TCR enhances the reduction of APL.
2. The AVD is 0.3445 p.u. (in case 14) but it is 0.32201 p.u. (in case 17). It shows the application of TSC-TCR has reduced AVD too.

Table 13
Simulation of a TSC-TCR based system employing COMMKE (single objective) with time-varying demand and unknown renewable power.

Scenario	Loading percentage	WP (MW)	PV Power (MW)	Scenario probability	Case 10 APL (MW)	Case 11 AVD (p.u.)
1	60	75	0	0.0417	0.823	0.0684
2	60	75	0	0.0417	0.831	0.0701
3	70	74.9262	0	0.0417	1.029	0.0774
4	70	67.3465	0	0.0417	1.128	0.0755
5	70	61.5781	0	0.0417	1.291	0.0685
6	80	49.9252	3.0649	0.0417	2.056	0.0872
7	80	44.2696	4.8102	0.0417	2.082	0.0753
8	90	39.6554	27.2938	0.0417	2.761	0.0848
9	90	32.7317	38.2988	0.0417	2.232	0.0875
10	90	26.9625	44.9323	0.0417	3.016	0.0901
11	100	27.48	49.8869	0.0417	4.031	0.1234
12	110	21.193	50	0.0417	5.861	0.1467
13	110	16.0633	50	0.0417	6.069	0.1477
14	100	14.1525	50	0.0417	4.815	0.1308
15	100	10.1758	40.688	0.0417	5.258	0.1398
16	90	5.0391	37.7282	0.0417	4.222	0.0897
17	90	1.3517	34.7949	0.0417	5.033	0.0905
18	100	9.6658	20.3495	0.0417	6.504	0.1276
19	110	9.02	7.2884	0.0417	10.023	0.1465
20	110	3.8795	0	0.0417	10.759	0.1486
21	110	20.5581	0	0.0417	10.021	0.1438
22	100	25.6863	0	0.0417	6.317	0.1223
23	90	39.1529	0	0.0417	3.748	0.0923
24	70	57.6213	0	0.0417	1.059	0.0781
Case 10:					Case 11:	
EAPL = 4.2104 MW					EAVD = 0.1048 p.u.	

Table 14
Simulation of a TSC-TCR based system utilizing COMMKE (Multi-objective- Case 12) with time-varying demand and renewable power.

Scenario	Loading percentage	WP (MW)	PV Power (MW)	Scenario probability	Objective value (Case 12)	APL (MW)	AVD (p.u.)
1	60	75	0	0.0417	1.658	0.906	0.0752
2	60	75	0	0.0417	1.645	0.902	0.0743
3	70	74.9262	0	0.0417	2.045	1.214	0.0831
4	70	67.3465	0	0.0417	2.126	1.325	0.0801
5	70	61.5781	0	0.0417	1.984	1.273	0.0711
6	80	49.9252	3.0649	0.0417	3.44	2.461	0.0979
7	80	44.2696	4.8102	0.0417	3.213	2.359	0.0854
8	90	39.6554	27.2938	0.0417	4.095	2.952	0.1143
9	90	32.7317	38.2988	0.0417	4.266	3.112	0.1154
10	90	26.9625	44.9323	0.0417	4.376	3.217	0.1159
11	100	27.48	49.8869	0.0417	5.975	4.653	0.1322
12	110	21.193	50	0.0417	8.37	6.769	0.1601
13	110	16.0633	50	0.0417	8.944	7.376	0.1568
14	100	14.1525	50	0.0417	6.632	5.344	0.1288
15	100	10.1758	40.688	0.0417	7.709	6.232	0.1477
16	90	5.0391	37.7282	0.0417	6.035	5.068	0.0967
17	90	1.3517	34.7949	0.0417	6.515	5.623	0.0892
18	100	9.6658	20.3495	0.0417	8.506	7.217	0.1289
19	110	9.02	7.2884	0.0417	13.1	11.568	0.1532
20	110	3.8795	0	0.0417	12.608	11.007	0.1601
21	110	20.5581	0	0.0417	11.953	10.341	0.1612
22	100	25.6863	0	0.0417	8.445	7.123	0.1322
23	90	39.1529	0	0.0417	5.742	4.675	0.1067
24	70	57.6213	0	0.0417	2.184	1.341	0.0843
EAPL: 4.7562 MW					EAVD: 0.1147 p.u.		

3. when multi-objective cases 15 & 18 are executed the value of APL & AVD, respectively, are 155.897 (MW), 0.4908 p.u. (case 15) and 153.897 (MW), 0.4781 p.u. (case 18). It again shows that use of TSC-TCR helps to minimize APL & AVD.

The cases 19–21 are conducted in varying load demand situation. Here, 24 scenarios are developed and shown in the test framework, Table 10 are taken into account. The results of cases 19–20 which are single objective cases, are placed in Table 17. Applying

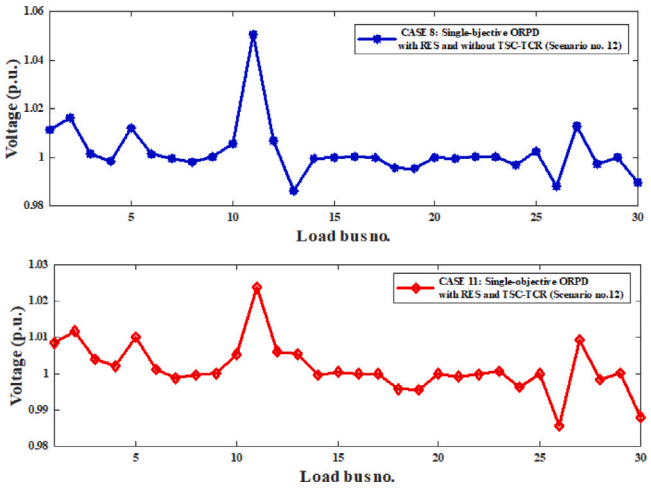

Fig. 9. Voltage deviations of the load bus for cases 8 and 11 in the for estimated scenarios 12.

Table 15
An overview of IEEE 118- bus System under study.

Items	Quantity	Details
Buses	118	[62]
Branches	186	
		Buses:69 (swing), 1,4,6, 8,10,12,15,18,19,24,25,26.27,31,32,34,36,40,42,46,49,54,55,56,59,61,62,65,66, 69,70,72,73,74,76,77,80,85,87,89,90,91,92,99,100,103,104,105,107,110,111,112,113 and 116
Wind generators (WG)	1	Bus:25
Solar PV unit (SPV)	1	Bus:40
Tap changing transformer	9	Branches:(8–5), (26–35),(30–17),(38–37),(63–59),(64–61),(65–66),(68–69) and (81–80)
Control variables	77	voltages(54)+transformer tap settings (9)+shunt capacitor (14)
Load demand		4242.0 MW, 1439.0 MVAr
Range of load bus voltage	64	[0.95–1.05]p.u.
TSC-TCR	1	Branch location and rating optimized
Compensation devices	14	Buses:5,34,37,44,45,46,48,74,79,82,83,105,107 and 110

COMMKE, as per Eqs. (28) & (29), respectively, the computed values of EAPL (case 19) is 109.6371 MW and the value of EAVD 0.7657 (case 20). These results are taken from all the developed 24 scenarios and their probabilities into account. Finally, the results of the scenario based multi-objective case *i.e.* case 21 are displayed in Table 18 where the EAPL & EAVD are computed as 110.1346 MW & 0.7742 p.u., respectively.

The same cases (*i.e.* 13–20) are experimented using MMKE & DTBO algorithms to compare the degree of effectiveness of COMMKE in contrast to MMKE & DTBO schemes. Every cases are experimented by 30 trials and from the outcomes, statistical record has been created and shown in Table 19. To make these database easy to access, box plots have been shown in Fig. 10 for cases 13–15. The significant points which can be noted from these statistical database & the box plots are:

1. For all the considered cases (*i.e.* 13–20), most fit objective function values are generated through the application of COMMKE.
2. COMMKE not only gives the best optimal values of the goal function but also produces the narrowest spread of the goal function values for 30 unbiased trials with respect to MMKE & DTBO.

These observations ensure the excellency and the regularity of the COMMKE algorithm.

In addition to these statistical records, the one way ANOVA tests have also been carried out in this work and the results are presented in Fig. 11 & in Table 20 for cases 16–18. The error bar plots are provided for cases 19–20 in Fig. 12. The simulation results clearly shows the superiority of COMMKE over its other rivalry.

6. Conclusions

Utilizing COMMKE across three test settings – illustrated in the study's three test frameworks – the ORPD problem has been addressed in the current work. The first framework looks at a traditional network with an IEEE 30-bus setup, whereas the second framework uses a traditional network accompanied with RESs. In the third test framework, simulation on IEEE 118 bus system is considered and the conventional network is also modified using FACTs tool and RESs. While the later phases of the study use a scenario creation & lowering approach to handle the stochasticity of load demand and RESs, its earlier phases are conducted in a deterministic context. Scenarios have been created using MCS, and the number of situations has been reduced to a tolerable

Table 16
Simulation results of case studies with fixed loading (100%) without & with FACTS for the adapted IEEE 118 bus system.

	Control parameter	Case 13	Case 14	Case 15	Case 16	Case 17	Case 18		Control parameter	Case 13	Case 14	Case 15	Case 16	Case 17	Case 18
V_{Min} = 0.94 (p.u.) V_{max} = 1.06 (p. u.)								V_{Min} = 0.94 (p.u.) V_{max} = 1.06 (p. u.)							
Generators' voltage (p.u.)	V1	0.988	1.0349	1.0305	1.0946	0.9652	1.0389	Generators' voltage (p.u.)	V99	1.0121	1.0091	1.0219	0.977	1.0369	1.0947
	V4	1.0426	1.0197	1.0445	0.9988	1.0165	0.9644		V100	1.0661	0.9787	1.0274	0.9557	1.0013	1.0548
	V6	1.0171	0.9802	1.0103	1.0232	0.9639	1.0535		V103	1.0383	0.961	1.0321	1.0329	0.9996	0.9897
	V8	1.0607	1.0592	1.0602	1.0687	1.0081	1.0369		V104	1.076	0.953	1.0934	1.0127	1.002	1.0193
	V10	1.0059	1.037	1.0812	1.0649	1.0292	1.0831		V105	1.015	1.0517	1.0772	1.0337	1.0078	1.0208
	V12	1.0395	1.029	1.0305	1.0351	1.0429	0.9777		V107	0.971	1.0416	1.0027	1.0201	0.9639	0.9922
	V15	1.0232	1.0639	0.9842	0.9695	0.9788	1.0314		V110	1.0024	1.0155	1.0901	0.9779	0.982	0.9696
	V18	1.0206	1.0792	1.0972	1.0221	0.9955	1.0622		V111	1.0949	0.9736	1.0148	1.0951	0.9763	0.9805
	V19	0.9682	1.0601	1.0393	0.9535	0.9917	1.0015		V112	1.0756	1.0201	1.0142	0.9691	1.0123	0.9717
	V24	0.9741	0.9993	1.0959	1.0596	0.9762	1.0238		V113	1.0852	0.9867	1.0782	0.9734	1.0567	1.0532
	V25	1.0437	1.0722	1.0979	1.0331	1.0103	0.965		V116	1.0657	0.9801	1.074	1.0874	1.0623	1.0554
	V26	1.0386	1.0686	0.9868	1.0425	1.0507	1.0325	TC_{Min} = 0.9 TC_{max} = 1.1							
	V27	1.0446	1.0655	1.0575	1.0416	0.9895	0.9809	Transformers' tap setting	T8	0.9609	1.0782	0.9533	0.9735	0.9581	1.0615
	V31	1.0289	0.9539	1.0663	1.0591	1.0106	0.9866		T32	1.0814	0.9098	0.9414	1.0641	0.9297	0.9008
	V32	1.0181	1.0278	1.0578	0.9683	1.03	0.9877		T36	1.0029	1.0912	0.9071	1.0773	1.0344	0.969
	V34	1.0121	1.0982	1.0758	1.0113	1.0434	0.9856		T51	0.9308	0.988	1.0199	0.9117	1.0378	0.9047
	V36	1.0715	1.0479	1.0729	0.9992	0.9812	1.058		T93	1.0748	0.9205	1.0837	0.9864	0.9722	1.0804
	V40	1.0451	1.0863	1.0386	0.9532	1.0468	1.0647		T95	1.083	1.0933	1.0415	0.9988	0.9045	1.0154
	V42	0.9572	1.0503	1.088	0.9622	1.0259	1.0249		T102	0.908	0.9748	1.0927	0.9609	0.9428	1.0253
	V46	1.0233	0.9503	1.0942	0.9813	0.9525	0.9661		T107	1.0424	1.0937	0.9108	1.0846	1.0296	1.0261
	V49	0.9938	1.0068	1.0354	1.0462	1.0297	1.0698		T127	0.9915	0.9163	0.9081	0.9947	1.0393	1.0039
	V54	1.0151	1.0496	1.0097	1.0182	1.0875	1.0639	QC_{Min} = 0 MVAr QC_{max} = 30 MVAr							
	V55	1.0514	1.054	1.071	1.02	1.0236	1.084	VAR injection (MVAr)	QC5	27.76	19.68	17.1	14.56	22.31	12.22
	V56	0.9929	1.0536	1.0438	0.9956	1.0652	1.0596		QC34	13.91	15.17	17.97	28.19	9.54	27.62
	V59	1.0656	1.092	1.0296	1.0189	0.9799	0.9599		QC37	23.44	14.28	0.15	18.13	26.91	16.1
	V61	0.9804	1.0907	0.9716	0.9936	1.0532	0.9698		QC44	29.99	16.92	22.82	0.29	16.76	9.99
	V62	1.0415	1.0386	0.9528	0.9789	0.9963	1.0353		QC45	12.58	6.65	7.27	13.94	0.7	4.69
	V65	1.0246	1.0381	0.9663	1.0769	1.0373	1.0076		QC46	22.34	0.59	28.65	21.51	1.51	0.73
	V66	1.0116	0.9747	1.0753	1.0019	0.9789	1.0327		QC48	23.15	18.25	10.39	21.43	25.49	3.03
	V69	1.0093	1.0574	0.9975	1.0485	1.0614	0.9698		QC74	7.85	5.62	10.91	0.62	10.79	24.33
	V70	0.9896	1.092	0.9819	0.9873	1.0544	0.96		QC79	28.52	8.74	8.55	17.95	8.6	29.69
	V72	0.955	1.0998	1.0879	1.0898	0.9852	0.989		QC82	2.45	10.42	3.69	16.28	15.43	6.51
	V73	1.0405	1.0215	1.0777	0.96	1.0142	0.9586		QC83	11.36	20.76	23.39	0.24	4.43	13.08
	V74	1.0818	1.0337	0.9865	1.0295	1.062	1.0246		QC105	1.68	27.33	8.36	10.87	29.63	28.67
	V76	1.0774	1.0652	1.0536	1.0401	1.0759	1.042		QC107	23.67	1.89	10.44	6.98	2.32	0.89
	V77	1.0163	0.999	0.9829	0.998	0.989	1.0444		QC110	5.22	4.99	1.09	4.71	7.44	7.89
	V80	0.9816	1.0984	1.0053	1.0421	0.9725	1.076	Optimal location of TSC-TCR					55	75	104
	V85	0.981	0.9976	1.0787	1.0178	1.0664	1.0139	QTSC-TCR(MVAr) (Min:Max: −10:20)					18.908	17.7785	15.896
	V87	1.0277	0.9691	1.0229	1.018	0.9721	1.0767	QTSC-TCR(MVAr) (Min:Max: −10:20)					18.908	17.7785	15.896
	V89	1.0402	1.0737	1.0857	1.0468	1.0561	1.0394	APL(MW)		**123.786**	167.876	**155.897**	**122.453**	161.098	**153.897**
	V90	0.9887	0.961	1.0267	1.0288	1.043	1.0101	AVD (p.u.)		0.5578	**0.3445**	**0.4908**	0.5223	**0.32201**	**0.4781**
	V91	1.0087	1.0408	1.0727	0.9522	1.0185	0.9926	L-index		0.987	0.897	0.876	0.898	0.7865	0.869
	V92	1.0418	1.0338	1.0274	0.9878	1.0968	1.0352								

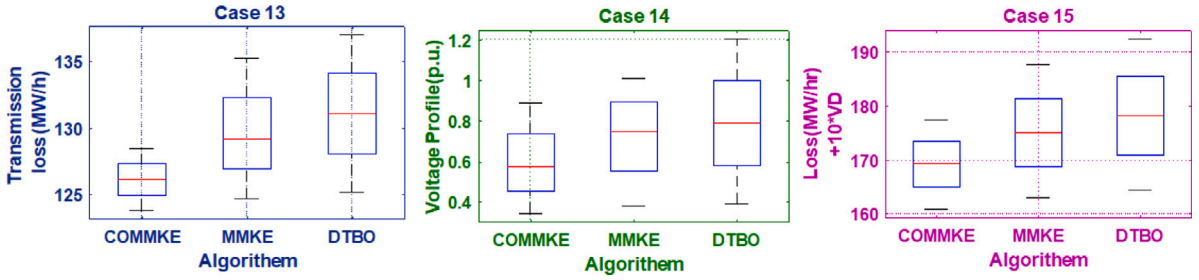

Fig. 10. Box plots for cases 13, 14 & 15.

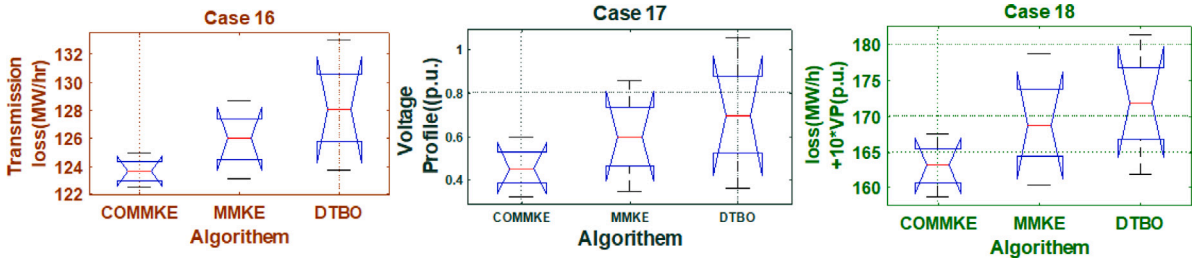

Fig. 11. Graphically, ANOVA results for cases 16, 17 & 18.

Table 17
Single-objective ORPD evaluted cases with time-varying demand and uncertain renewable power with TSC-TCR (IEEE 118 Bus system).

Scenario	% Loading	WP1 (MW) at bus 25	PV Power (MW) at bus 40	Scenario probability Δ_{sc}	Scenario based Case 19 APL (MW)	Scenario based Case 20 AVD (p.u.)
1	60	75	0	0.0417	76.4537	0.6894
2	60	75	0	0.0417	76.8930	0.6889
3	70	74.9262	0	0.0417	83.7843	0.7089
4	70	67.3465	0	0.0417	82.6630	0.7100
5	70	61.5781	0	0.0417	81.8934	0.7099
6	80	49.9252	3.0649	0.0417	94.5632	0.7209
7	80	44.2696	4.8102	0.0417	93.6748	0.7217
8	90	39.6554	27.2938	0.0417	102.6744	0.7584
9	90	32.7317	38.2988	0.0417	103.4537	0.7689
10	90	26.9625	44.9323	0.0417	104.5640	0.7701
11	100	27.48	49.8869	0.0417	125.6780	0.7991
12	110	21.193	50	0.0417	131.5634	0.8209
13	110	16.0633	50	0.0417	134.8902	0.8301
14	100	14.1525	50	0.0417	126.7843	0.8001
15	100	10.1758	40.688	0.0417	125.9085	0.8067
16	90	5.0391	37.7282	0.0417	110.6730	0.7789
17	90	1.3517	34.7949	0.0417	111.6998	0.7800
18	100	9.6658	20.3495	0.0417	125.9873	0.7999
19	110	9.02	7.2884	0.0417	135.7840	0.8205
20	110	3.8795	0	0.0417	137.5634	0.8190
21	110	20.5581	0	0.0417	135.7840	0.8234
22	100	25.6863	0	0.0417	126.9040	0.7989
23	90	39.1529	0	0.0417	113.7850	0.7489
24	70	57.6213	0	0.0417	85.5638	0.6877
		Case 19:			Case 20:	
		EAPL = **109.6371 MW**			EAVD = **0.7657** p.u.	

Table 18
Multi-objective ORPD with time-varying demand and uncertain renewable power with TSC-TCR (IEEE 118 bus system).

Scenario	Loading percentage	WP (MW)	PV Power (MW)	Scenario probability	Objective value (Case 21)	APL (MW)	AVD (p.u.)
1	60	75	0	0.0417	76.999	0.6994	83.9927
2	60	75	0	0.0417	77.564	0.7011	84.5754
3	70	74.9262	0	0.0417	84.400	0.7178	91.5781
4	70	67.3465	0	0.0417	83.068	0.7199	90.2667
5	70	61.5781	0	0.0417	82.453	0.7189	89.6421
6	80	49.9252	3.0649	0.0417	94.991	0.7289	102.2798
7	80	44.2696	4.8102	0.0417	94.010	0.7289	101.2988
8	90	39.6554	27.2938	0.0417	102.981	0.7675	110.6557
9	90	32.7317	38.2988	0.0417	103.888	0.7897	111.7849
10	90	26.9625	44.9323	0.0417	105.290	0.7799	113.0893
11	100	27.48	49.8869	0.0417	125.778	0.8100	133.8784
12	110	21.193	50	0.0417	132.011	0.8267	140.2781
13	110	16.0633	50	0.0417	135.221	0.8389	143.6099
14	100	14.1525	50	0.0417	126.990	0.8103	135.0934
15	100	10.1758	40.688	0.0417	127.009	0.8111	135.1201
16	90	5.0391	37.7282	0.0417	111.452	0.7810	119.2621
17	90	1.3517	34.7949	0.0417	112.445	0.7878	120.3233
18	100	9.6658	20.3495	0.0417	126.209	0.8102	134.3111
19	110	9.02	7.2884	0.0417	135.991	0.8277	144.2678
20	110	3.8795	0	0.0417	137.893	0.8234	146.1273
21	110	20.5581	0	0.0417	136.109	0.8288	144.3972
22	100	25.6863	0	0.0417	127.454	0.8104	135.5577
23	90	39.1529	0	0.0417	114.564	0.7578	122.1423
24	70	57.6213	0	0.0417	86.347	0.6908	93.2552
		EAPL: **110.1346 MW**				EAVD: **0.7742** p.u.	

amount using BRA. The relevant PDFs of load demand and RESs are also taken into account in this regard. The first goal of the study is to reduce AVD & APL. independently. The second aim is to reduce AVD & APL together as a multi-objective. Two runs of the experiments are conducted in each test setting, one with and one without TSC-TCR consideration.

Table 19
Statistical comparison (30 trials) among various algorithms for IEEE 118 bus system for solving cases 13 to 20.

Case		COMMKE	MMKE	DTBO	Case		COMMKE	MMKE	DTBO
	Best (min)	**123.786**	**124.674**	**125.101**		Best (min)	**0.32201**	**0.3452**	**0.3611**
	Mean (average)	125.998	129.024	131.002		Mean (average)	0.4401	0.5895	0.6892
Case 13	Median	126.123	129.422	131.234	Case 17	Median	0.4673	0.6121	0.6998
	Worst (max)	128.452	135.228	136.996		Worst (max)	0.5982	0.8564	1.0562
	Standard deviation	2.434	4.563	5.564		Standard deviation	0.1153	0.2435	0.3234
	Best (min)	**0.3445**	**0.3787**	**0.388**		Best (min)	**158.678**	**160.324**	**161.897**
	Mean (average)	0.5623	0.7234	0.7829		Mean (average)	162.679	168.453	171.784
Case 14	Median	0.5891	0.7782	0.8011	Case 18	Median	163.556	169.119	172.078
	Worst (max)	0.8927	1.0126	1.2023		Worst (max)	167.662	178.673	181.436
	Standard deviation	0.2343	0.3563	0.4452		Standard deviation	3.892	7.553	9.706
	Best (min)	**160.805**	**162.893**	164.271		Best (min)	**109.6371**	**110.574**	**113.463**
	Mean (average)	168.892	174.884	177.783		Mean (average)	110.342	112.764	116.998
Case 15	Median	169.881	175.334	178.662	Case 19	Median	110.897	112.988	117.231
	Worst (max)	177.443	187.673	192.435		Worst (max)	111.908	115.234	120.786
	Standard deviation	7.537	11.437	13.425		Standard deviation	1.003	2.164	3.563
	Best (min)	**122.453**	**123.177**	**123.763**		Best (min)	**0.7657**	**0.8674**	**0.9831**
	Mean (average)	123.546	125.876	127.896		Mean (average)	0.8766	1.178	1.189
Case 16	Median	123.786	126.117	128.227	Case 20	Median	0.8977	1.234	1.277
	Worst (max)	125.002	128.667	133.009		Worst (max)	1.008	1.563	1.897
	Standard deviation	1.024	2.436	4.015		Standard deviation	0.1145	0.2563	0.3134

Table 20
ANOVA results for cases 16, 17 & 18.

Case 16					
Source	SS	df	MS	F	Prob>F
Columns	40.987	2	20.4937	3.01	0.0998
Error	61.29	9	6.81		
Total	102.278	11			
Case 17					
Source	SS	df	MS	F	Prob>F
Columns	0.12097	2	0.06048	1.32	0.3134
Error	0.41131	9	0.0457		
Total	0.53228	11			
Case 18					
Source	SS	df	MS	F	Prob>F
Columns	157.264	2	78.632	1.77	0.2255
Error	400.815	9	44.535		
Total	558.079	11			

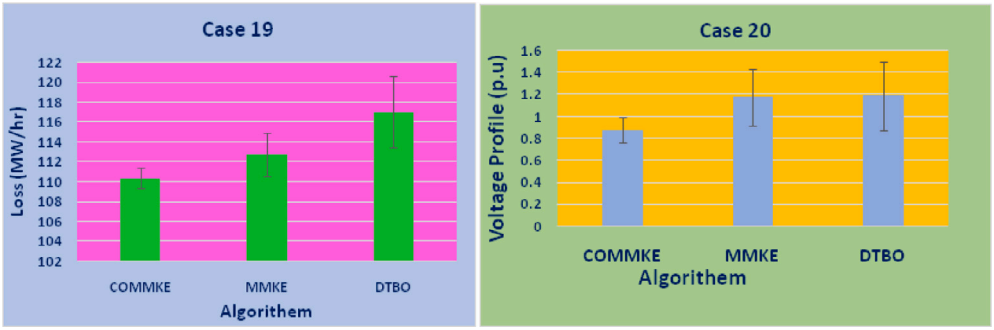

Fig. 12. Error-bar Plots for cases 19 & 20.

The experimental findings demonstrate that COMMKE performs better than contemporary optimization algorithms in test scenarios where volatility predominates, as well as in deterministic experimental setups. It has also been confirmed that all network limits remain in place and are maintained within the predefined parameters. This effort has produced an interesting finding: using TSC-TCR in ORPD problems is very beneficial for reducing APL and AVD. The remarkable efficacy of TSC-TCR remains true for both fixed uncertain loading cases. Higher ordered IEEE standard networks *i.e.* IEEE 118 bus system when tested the performance of

COMMKE is till significantly good. The degree of superiority of the COMMKE over other algorithms is well judged using statistical records, box plots, error bar diagrams, ANOVA tables & ANOVA figures.. Future research could be done with a greater variety of objectives and their combinations.

Ethical approval

This article does not contain any studies with human participants or animals performed by any of the authors.

Funding

No funding.

Declaration of competing interest

The authors declare that they have no known competing financial interests or personal relationships that could have appeared to influence the work reported in this paper.

Data availability

Data will be made available on request.

References

[1] Abul'Wafa Ahmed R. Optimization of economic/emission load dispatch for hybrid generating systems using controlled Elitist NSGA-II. Electr Power Syst Res 2013;105:142–51.
[2] Fotis Georgios, Vita Vasiliki, Maris Theodoros I. Risks in the European transmission system and a novel restoration strategy for a power system after a major blackout. Appl Sci 2023;13(1):83.
[3] Muhammad Yasir, Khan Rahimdad, Raja Muhammad Asif Zahoor, Ullah Farman, Chaudhary Naveed Ishtiaq, He Yigang. Solution of optimal reactive power dispatch with FACTS devices: A survey. Energy Rep 2020;6:2211–29.
[4] Saddique Muhammad Shahzar, Bhatti Abdul Rauf, Haroon Shaikh Saaqib, Sattar Muhammad Kashif, Amin Salman, Sajjad Intisar Ali, et al. Solution to optimal reactive power dispatch in transmission system using meta-heuristic techniques status and technological review. Electr Power Syst Res 2020;178:106031.
[5] Radosavljević Jordan. Metaheuristic optimization in power engineering. IET; 2018.
[6] Rajan Abhishek, Malakar Tanmoy. Exchange market algorithm based optimum reactive power dispatch. Appl Soft Comput 2016;43:320–36.
[7] Jangir Pradeep, Parmar Siddharth A, Trivedi Indrajit N, Bhesdadiya RH. A novel hybrid particle swarm optimizer with multi verse optimizer for global numerical optimization and optimal reactive power dispatch problem. Eng Sci Technol Int J 2017;20(2):570–86.
[8] Radosavljević Jordan, Jevtić Miroljub, Milovanović Miloš. A solution to the ORPD problem and critical analysis of the results. Electr Eng 2018;100:253–65.
[9] Roy Ranjit, Das Tanmay, Mandal Kamal Krishna. Optimal reactive power dispatch using a novel optimization algorithm. J Electr Syst Inf Technol 2021;8(1):1–24.
[10] Oda Eyad S, Hamed Amal M Abd El, Ali Abdelfatah, Elbaset Adel A, Sattar Montaser Abd El, Ebeed Mohamed. Stochastic optimal planning of distribution system considering integrated photovoltaic-based DG and DSTATCOM under uncertainties of loads and solar irradiance. IEEE Access 2021;9:26541–55.
[11] Venkatesh SV, Liu W-HE, Papalexopoulos Alex D. A least squares solution for optimal power flow sensitivity calculation. IEEE Trans Power Syst 1992;7(3):1394–401.
[12] Granville Sergio. Optimal reactive dispatch through interior point methods. IEEE Trans Power Syst 1994;9(1):136–46.
[13] Wu Yu-Chi, Debs Atif S, Marsten Roy E. A direct nonlinear predictor-corrector primal-dual interior point algorithm for optimal power flows. IEEE Trans Power Syst 1994;9(2):876–83.
[14] Lee KY, Park YM, Ortiz JL. A united approach to optimal real and reactive power dispatch. IEEE Trans Power Appar Syst 1985;104(5):1147–53.
[15] Mangoli Maurice K, Lee Kwang Y, Park Young Moon. Optimal real andreactive power control using linear programming. Electr Powersyst Res 1993;26(1):1–10.
[16] Kirschen Daniel S, Van Meeteren Hans P. MW/voltage control in a linear programming based optimal power flow. IEEE Trans Power Syst 1988;3(2):481–9.
[17] Quintana VH, Santos-Nieto M. Reactive-power dispatch by successive quadratic programming. IEEE Trans Energy Convers 1989;4(3):425–35.
[18] Nanda Janardan, Kothari Dwarkadas P, Srivastava Suresh C. New optimal power-dispatch algorithm using Fletcher's quadratic programming method. IEE Proc C 1989;136(3):153–61.
[19] Grudinin N. Reactive poweroptimization using successive quadratic programming method. IEEE Trans Power Syst 1998;13(4):1219–25.
[20] Houssein Essam H, Mahdy Mohamed A, Blondin Maude J, Shebl Doaa, Mohamed Waleed M. Hybrid slime mould algorithm with adaptive guided differential evolution algorithm for combinatorial and global optimization problems. Expert Syst Appl 2021;174:114689.
[21] Tudose Andrei M, Irina I, Picioroaga Dorian O, Sidea Constantin Bulac. Solving single- and multi-objective optimal reactive power dispatch problems using an improved salp swarm algorithm. Energies 2021;14(5).
[22] Sulaiman Mohd Herwan, Mustaffa Zuriani, Saari Mohd Mawardi, Daniyal Hamdan, Daud Mohd Razali, Razali Saifudin, et al. Barnacles mating optimizer: a bio-inspired algorithm for solving optimization problems. In: 2018 19th IEEE/aCIS international conference on software engineering, artificial intelligence, networking and parallel/distributed computing. IEEE; 2018, p. 265–70.
[23] Li Shimin, Chen Huiling, Wang Mingjing, Heidari Ali Asghar, Mirjalili Seyedali. Slime mould algorithm: A new method for stochastic optimization. Future Gener Comput Syst 2020;111:300–23.
[24] Nuaekaew Kasem, Artrit Pramin, Pholdee Nantiwat, Bureerat Sujin. Optimal reactive power dispatch problem using a two-archive multi-objective grey wolf optimizer. Expert Syst Appl 2017;87:79–89.
[25] Hosseini-Hemati Saman, Sheisi Gholam Hossein, Karimi Shahram. Allocation-based optimal reactive power dispatch considering polynomial load model using improved grey wolf optimizer. Iran J Sci Technol Trans Electr Eng 2021;45:921–44.
[26] Ettappan M, Vimala V, Ramesh S, Kesavan V Thiruppathy. Optimal reactive power dispatch for real power loss minimization and voltage stability enhancement using Artificial Bee Colony Algorithm. Microprocess Microsyst 2020;76:103085.

[27] Radosavljević J, Jevtić M, Milovanović M. A solution to the ORPD problem and critical analysis of the results. Electr Eng 2018;253–65.
[28] Singh Rudra Pratap, Mukherjee V, Ghoshal SP. Optimal reactive power dispatch by particle swarm optimization with an aging leader and challengers. Appl Soft Comput 2015;29:298–309.
[29] Mehdinejad Mehdi, Mohammadi-Ivatloo Behnam, Dadashzadeh-Bonab Reza, Zare Kazem. Solution of optimal reactive power dispatch of power systems using hybrid particle swarm optimization and imperialist competitive algorithms. Int J Electr Power Energy Syst 2016;83:104–16.
[30] Basu M. Quasi-oppositionaldifferential evolution for optimal reactive power dispatch. Int Electr Power Energy Syst 2016;78:29–40.
[31] Al Misba Walid, Ndoye Mandoye, Arif Md Arifin, Murphy Gregory V. Multi-objectiveoptimal reactive power dispatch using modified game theory. In: 2017 NorthAmerican power symposium. IEEE; 2017, p. 1–6.
[32] Shareef SKMahammad, Rao R Srinivasa. Optimal reactivepower dispatch under unbalanced conditions using hybrid swarm intelligence. Comput Electr Eng 2018;69:183–93.
[33] De Mala, Goswami Swapan K. Optimal reactivepower procurement with voltage stability consideration in deregulated powersystem. IEEE Trans Power Syst 2014;29(5):2078–86.
[34] Mandal Barun, Roy Provas Kumar. Optimal reactivepower dispatch using quasi-oppositional teaching learning based optimization. Int J Electr Power Energy Syst 2013;53:123–34.
[35] Ghasemi Mojtaba, Taghizadeh Mahdi, Ghavidel Sahand, Aghaei Jamshid, Abbasian Abbas. Solving optimal reactive power dispatch problem using a novel teaching–learning-based optimization algorithm. Eng Appl Artif Intell 2015;39:100–8.
[36] Mouwafi RAEMT. Optimal reactivepower dispatch using ant colony optimization algorithm. Electr Eng 2011;93:103–16.
[37] Gupta Sushil Kumar, Kumar Lalit, Kar Manoj Kumar, Kumar Sanjay. Optimal reactive power dispatch under coordinated active and reactive load variations using FACTS devices. Int J Syst Assur Eng Manag 2022;13(5):2672–82.
[38] Mehdinejad Mehdi, Mohammadi-Ivatloo Behnam, Dadashzadeh-Bonab Reza, Zare Kazem. Solution of optimalreactive power dispatch of power systems using hybrid particle swarmoptimization and imperialist competitive algorithms. Int J Electr Power Energy Syst 2016;83:104–16.
[39] Biswas Partha P, Suganthan PN, Mallipeddi R, Amaratunga Gehan AJ. Optimal reactive power dispatch with uncertainties in load demand and renewable energy sources adopting scenario-based approach. Appl Soft Comput 2019;75:616–32.
[40] Habib Khan Noor, Jamal Raheela, Ebeed Mohamed, Kamel Salah, Zeinoddini-Meymand Hamed, Zawbaa Hossam M. Adopting Scenario-Based approach to solve optimal reactive power Dispatch problem with integration of wind and solar energy using improved Marine predator algorithm. Ain Shams Eng J 2022;13(5):101726.
[41] Zhang Meng, Li Yang. Multi-objective optimal reactive power dispatch of power systems by combining classification-based multi-objective evolutionary algorithm and integrated decision making. IEEE Access 2020;8:38198–209.
[42] Ela AA Abou El, Abido MA, Spea SR. Differential evolution algorithm for optimal reactive power dispatch. Electr Power Syst Res 2011;81(2):458–64.
[43] Suresh V, Kumar S Senthil. Optimal reactive power dispatch for minimization of real power loss using SBDE and DE-strategy algorithm. J Ambient Intell Humaniz Comput 2020;1–15.
[44] Subbaraj P, Rajnarayanan PN. Optimal reactive power dispatch using self-adaptive real coded genetic algorithm. Electr Power Syst Res 2009;79(2):374–81.
[45] Ma JT, Lai LL. Application of genetic algorithm to optimal reactive power dispatch. IFAC Proc Vol 1995;28(10):571–6, 7th IFAC Symposium on Large Scale Systems: Theory and Applications 1995, London, UK, 11-13 July, 1995.
[46] Khazali AH, Kalantar M. Optimal reactive power dispatch based on harmony search algorithm. Int J Electr Power Energy Syst 2011;33(3):684–92.
[47] Abdelmoumene Messaoudi. Optimal reactive power dispatch solution using enhanced sine cosine optimization algorithm with selection operator. Int J Eng Res Afr 2020;51:29–44.
[48] Bhattacharya Aniruddha, Chattopadhyay Pranab Kumar. Solution of optimal reactive power flow using biogeography-based optimization. Int J Electr Comput Eng 2010;4(3):621–9.
[49] Shaw Binod, Mukherjee V, Ghoshal Sakti Prasad. Solution of optimal reactive power dispatch by an opposition-based gravitational search algorithm. In: Panigrahi Bijaya Ketan, Suganthan Ponnuthurai Nagaratnam, Das Swagatam, Dash Shubhransu Sekhar, editors. Swarm, evolutionary, and memetic computing. Cham: Springer International Publishing; 2013, p. 558–67.
[50] Nadimi-Shahraki Mohammad H, Taghian Shokooh, Zamani Hoda, Mirjalili Seyedali, Elaziz Mohamed Abd. MMKE: Multi-trial vector-based monkey king evolution algorithm and its applications for engineering optimization problems. PLoS One 2023;18(1):e0280006.
[51] Meng Zhenyu, Pan Jeng-Shyang. Monkey king evolution: a new memetic evolutionary algorithm and its application in vehicle fuel consumption optimization. Knowl-Based Syst 2016;97:144–57.
[52] Tizhoosh Hamid R. Opposition-based learning: a new scheme for machine intelligence. In: International conference on computational intelligence for modelling, control and automation and international conference on intelligent agents, web technologies and internet commerce, vol. 1. IEEE; 2005, p. 695–701.
[53] Paul Chandan, Roy Provas Kumar, Mukherjee V. Chaotic whale optimization algorithm for optimal solution of combined heat and power economic dispatch problem incorporating wind. Renew Energy Focus 2020;35:56–71.
[54] Chaurasiya Kumarshanu, Rajput Sagar, Parmar Sachin, Patel Abhishek. Reactive power management using TSC-TCR. IRJET 2018;5:1427–31.
[55] Rambabu M, Nagesh Kumar GV, Sivanagaraju S. Optimal power flow of integrated renewable energy system using a thyristor controlled SeriesCompensator and a grey-wolf algorithm. Energies 2019;12(11):2215.
[56] Duman Serhat, Li Jie, Wu Lei, Guvenc Ugur. Optimal power flow with stochastic wind power and FACTS devices: a modified hybrid PSOGSA with chaotic maps approach. Neural Comput Appl 2020;32:8463–92.
[57] Abdullah Muhammad, Javaid Nadeem, Khan Inam Ullah, Khan Zahoor Ali, Chand Annas, Ahmad Noman. Optimal power flow with uncertain renewable energy sources using flower pollination algorithm. In: Advanced information networking and applications: Proceedings of the 33rd international conference on advanced information networking and applications. Springer; 2020, p. 95–107.
[58] Tanabe Ryoji, Fukunaga Alex. Success-history based parameter adaptation for differential evolution. In: 2013 IEEE congress on evolutionary computation. IEEE; 2013, p. 71–8.
[59] Mukherjee Aparajita, Roy Provas Kumar, Mukherjee V. Transient stability constrained optimal power flow using oppositional krill herd algorithm. Int J Electr Power Energy Syst 2016;83:283–97.
[60] Ramalingam Rajakumar, Karunanidy Dinesh, Alshamrani Sultan S, Rashid Mamoon, Mathumohan Swamidoss, Dumka Ankur. Oppositional pigeon-inspired optimizer for solving the non-convex economic load dispatch problem in power systems. Mathematics 2022;10(18):3315.
[61] Growe-Kuska Nicole, Heitsch Holger, Romisch Werner. Scenario reduction and scenario tree construction for power management problems. In: 2003 IEEE Bologna power tech conference proceedings. 3, IEEE; 2003, p. 7.
[62] Gupta Sabyasachi, Sarkar Tushnik, Paul Chandan, Dutta Susanta, Roy Provas Kumar. Applicability of MMKE alongside statistical assessment in RESs and SVC-based power networks to solve the ORPD problem in load-varying scenarios. Electr Eng 2024;1–35.